29 Apr 1981, 1:30 pm - 5:00 pm

Free Field and Design Motions During Earthquakes

T. Iwasaki

Public Works Research Institute, Ministry of Construction, Tsukuba, Japan

Proceedings: First International Conference on Recent Advances in Geotechnical Earthquake Engineering and Soil Dynamics, April 26 - May 3, 1981, St. Louis, Missouri

Free Field and Design Motions During Earthquakes

T. Iwasaki, Head

Ground Vibration Division, Public Works Research Institute, Ministry of Construction, Tsukuba, Japan

SYNOPSIS Recent development of free field ground motions and structural design motions are described with emphasis on investigations done in Japan. The results of analyses of peak free field accelerations and frequency characteristics of response spectra are discussed. Also the recent topics of studies on ground motions including strong-motion earthquake instrument arrays and soil-structure interaction problems are described with use of the results of measurements of strong-motion earthquakes.

INTRODUCTION

For determining appropriate seismic effects to be considered in the design of civil engineering structures against earthquake disturbances, it is essential to assess intensities and characteristics of ground motions and structural responses during earthquakes. This paper reviews the recent development of studies on free field ground motions and structural motions during strong earthquakes. Although it primarily covers the results of relevant works performed in Japan, it also briefly summarizes some typical investigations done in the United States. This paper emphasizes fundamental research findings rather than practical design aspects.

PRESENT STATUS OF OBSERVATION OF STRONG-MOTION EARTHQUAKE

In Japan the installation of strong-motion accelerographs for engineering structures was initiated in 1953, after manufacturing of SMAC-type accelerographs was commenced. The observation network has gradually progressed with experiences of servere structural damages due to the Niigata Earthquake of 1964 and the Tokachi-oki Earthquake of 1968. At the present the number of

Table I Number of Strong-Motion Accelerographs (SMAC-Type)

Number of Accelerographs Installed at	At Structure	On Free Fields	Total
Buildings	424	48	472
Highway Bridges	89	79	168
Railways	38	57	95
Ports	5	51	56
Telephone Offices	94	0	94
Power Plants	27	11	38
Nuclear Power Plants	21	20	41
Dams	9	10	19
River & Coastal Dykes	15	28	43
Storage Tanks	3	4	7
Others (Tunnels, Subways, Pipelines, etc.)	5	10	15
Total	730	318	1,048

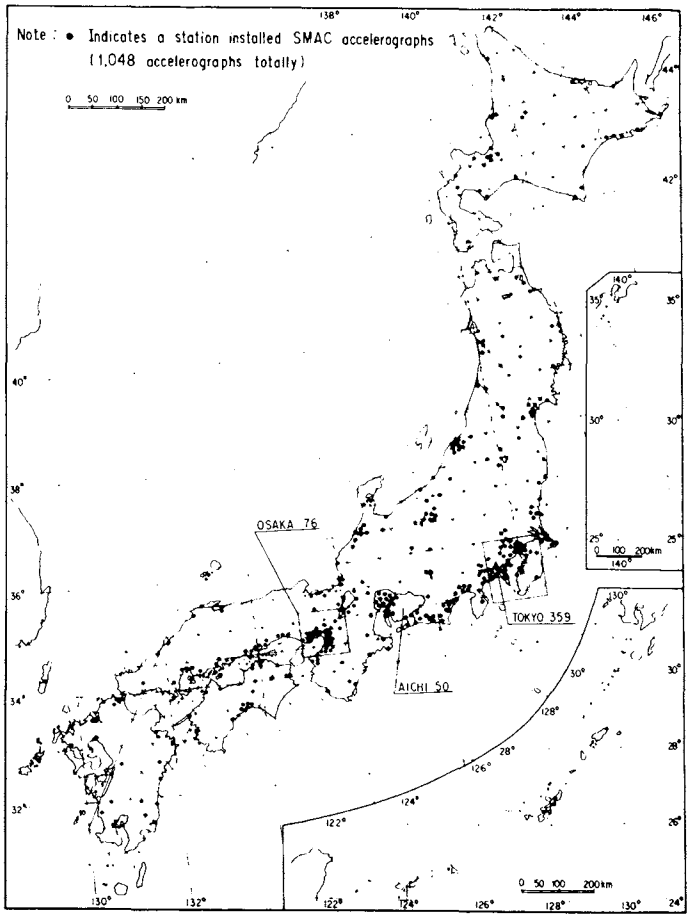

Fig. 1 Strong-Motion Observation Network in Japan as of March, 1976

strong-motion accelerographs is over 1,000, as shown in Table I and Fig.1. It is believed, however, that the same number of accelerographs is necessitated additionally, in order to obtain ample strong-motion records for major earthquakes which may take place at any areas of the country. Accelerographs installed on free field grounds are only about 30 % of the total, and the rest is on various engineering structures such as buildings, bridges, port and harbor structures, dams, etc. Most of accelerographs on free fields have been equipped in connection with bridges, ports and railways. Characteristics of typically used accelerographs are shown in Table II.

In addition to the stations with SMAC-type accelerographs, there are a number of stations where electromagnetic type seismographs are equipped. Furthermore, many of downhole accelerometers are also installed to measure dynamic behavior of subsoils during earthquakes.

Installation and maintenance of instruments are generally conducted by individual organizations such as the Ministry of Construction, the Ministry of Transport, the Japanese National Railways, Nippon Telegraph and Telephone Public Corporation, private companies, and so on. Records from the abovementioned instruments are collected and published periodically at several research institutes concerned. Digitization of major accelerograms is also conducted at the research institutes, such as PWRI, BRI and PHRI.

Table II Characteristics of Typical Strong-Motion Accelerographs

Characteristics	Type of Strong-Motion Accelerographs		
	SMAC-B (B_2)	SMAC-E (E_2)	SMAC-M
Component	2 Horizontal 1 vertical	ditto	ditto
Type	accelerograph	ditto	ditto
Natural period (sec)	0.1 (0.14)	0.05	450 (Hz)
Sensitivity (gals/mm)	25 (12.5)	200 (100)	1 (Volt/g)
Damping	Critical	60 % of critical	60 % of critical
Damping mechanism	Air piston	ditto	Electric
Recording range (gals)	10 - 1000 (6 - 500)	10 - 1000 (5 - 500)	5 - 1000
Recording speed	10 mm/sec	5 mm/sec (2.5)	47.5 mm/sec
Recording medium	Waxed paper	Scratch record film	Cassetee tape
Recording drive	Hand-wound spring moter	Micro-moter	Data recorder (FM recording)
Recording duration	3 min.	1.5 min.	3 min.
No. repeat cycles	5	More than 100 (200)	10
Starter	Elect. contact made by vertical motion	ditto	Elect. dynamic vertical pick-up
Period of starter pendulum (sec)	0.3	ditto	0.22
Starter threshold (gals)	10 (5)	10 (5)	5
Auxiliary starter	Mechanical, works at 100 gals	None	None
Time marking	1 sec.	0.5 sec.	0.01 sec.
Power supply	4 dry cells	10 dry cells	Ni-Cd cells
Size, overall (cm)	54 × 54 × 37	45 × 45 × 37	60 × 35.4 × 15.7
Weight (kg)	100	70	23

Status of strong-motion instrumental networks and records in U.S. is well summarized by Jennings and Helmberger (1978), together with discussions of some recent results in strong-motion seismology. From this about 850 accelerographs, 150 seismographs, and 25 peak recording accelerographs are maintained by several institutions. The installations in U.S. are much more concentrated on surface free fields comparing with the Japanese case.

ANALYSES OF PEAK ACCELERATION

A statistical analysis of acceleration records obtained on surface free fields in Japan, was attempted to quantitatively express characteristic variables of ground motions as functions of seismic conditions and soil properties at the observation sites. In the analysis were employed strong-motion records which were triggered during earthquakes with the magnitude (determined by the Japan Meteorological Agency) of 5.0 or higher and the hypocentral depth of 60 km or shallower, and which included at least one record with the peak acceleration of 50 gals or higher. Records with the peak acceleration less than 10 gals are excluded. The total number of the records is 301 (the number of components is 3 x 301 = 903) from 51 earthquakes.

Factors considered in the analysis are as follows :

(1) Seismic conditions : Magnitude M, epicentral distance Δ (km)

(2) Soil properties : Observation sites are classified into the following four groups depending on soil conditions

Group I : Rock
Group II : Diluvium
Group III : Alluvium (Except Group IV)
Group IV : Soft Alluvium

The definitions of the classification are shown in the bottom of Table VII in the following section.

(3) Characteristic variables of acceleration records :

(a) H_{max} (gals) : Absolute peak acceleration that is the larger value of two perpendicular horizontal motions

(b) T_1 (sec) : Period of vibration around the time when acceleration becomes H_{max}

(c) T_d (sec) : Duration of major motion

(d) $v = V_{max}/H_{max}$: Ratio of peak vertical acceleration (V_{max}) to H_{max}

(e) N_z : Number of zero-crossing during the time length of T_d

(f) $T_m = T_d / N_z$: Mean period during the time of T_d

The procedure and definition for determining the above characteristic variables are illustrated in Fig.2. Each of the characteristic variables (expressed as X below) was assumed to be represented by the following expression :

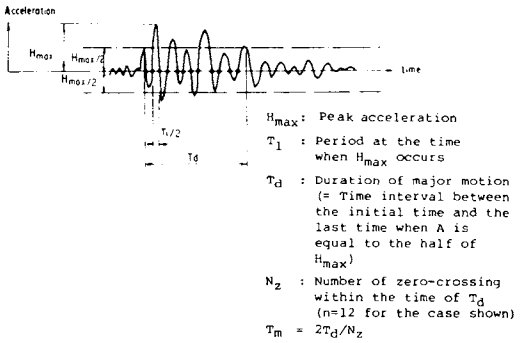

Fig. 2 Definition of Peak Acceleration, and Characteristic Variables of Strong-Motion Records

$$X = a \cdot 10^{bM} \Delta^{c} \qquad (1)$$

where a, b, and c are constants for each characteristic variable, and are depending on soil conditions.

Analyses were done for five different cases, namely the four groups of soil conditions plus the average soils of the entire data. In determining the expressions for H_{max}, the term of Δ in eq. (1) was substituted by $\Delta + \Delta_0$ where Δ_0 was taken as 0, 10, 20, 30, and 40 km. Table III indicates the distribution of the 301 records used in the analysis. Table IV shows formulated regression equations and multiple correlation coefficients. In the table are shown the results of three characteristic values H_{max}, T_d, and N_z for which multiple correlation coefficients were generally greater than 0.5. Because the correlation was the highest for the case of $\Delta_0 = 10$ km among the above five cases analyzed, H_{max} for the case of $\Delta_0 = 10$ km is shown in Table IV. Fig. 3 illustrates H_{max} for $\Delta_0 = 10$ km as functions of the magnitude M and the epicentral distance Δ, for the case of the average soils.

Table III Classification of 301 Strong-Motion Records Analyzed

Magnitude M	Soil Condition	Epicental Distance Δ (km) $20 < \Delta$	$20 \cdot \Delta < 60$	$60 \cdot \Delta < 120$	$120 \cdot \Delta < 200$	$200 \cdot \Delta$	Total	
5.0 ·M< 6.0	Rock	2	3				5	67
	Dil.	3	12	3			18	
	All.	4	16	5	2	2	29	
	Soft All.	2	5	7	1		15	
6.0 ·M< 6.5	Rock		3	6	3	1	13	81
	Dil.		7	8	2	1	18	
	All.		12	13	8	1	34	
	Soft All.		3	6	6	1	16	
6.5 ·M< 7.0	Rock		1	2	1		4	62
	Dil.		1	6	6		13	
	All.	1	5	10	10	1	27	
	Soft All.		1	4	9	4	18	
7.0 ·M< 7.5	Rock			1		3	4	41
	Dil.				2	12	14	
	All.				2	14	16	
	Soft All.			1	1	5	7	
7.5 ·M< 7.9	Rock				1	2	3	50
	Dil.				3	8	11	
	All.			2	6	16	24	
	Soft All.				1	11	12	
Total		12	69	74	64	82	301	

Note. 1) Numbers of records for four soil conditions are 29 for rock, 74 for diluvium, 130 for alluvium, and 68 for soft alluvium.

Table IV Regression Equations for H_{max}, T_d and N_z

Characteristic Value	Soil Condition	Empirical Equations	Multiple Correlation Coefficient r
H_{max} (gals)	Rock	$H_{max} = 46.0 \times 10^{0.208M} \times (\Delta+10)^{-0.686}$	0.48
	Dil.	$H_{max} = 24.5 \cdot 10^{0.333M} \times (\Delta+10)^{-0.924}$	0.59
	All.	$H_{max} = 59.0 \times 10^{0.261M} \times (\Delta+10)^{-0.886}$	0.62
	Soft All.	$H_{max} = 12.8 \times 10^{0.432M} \times (\Delta+10)^{-1.125}$	0.68
	Total	$H_{max} = 34.1 \times 10^{0.368M} \times (\Delta+10)^{-0.925}$	0.61
T_d (sec)	Rock	$T_d = 3.89 \times 10^{-4} \times 10^{0.466M} \times 0.589$	0.89
	Dil.	$T_d = 1.37 \times 10^{-2} \times 10^{0.262M} \times 0.485$	0.71
	All.	$T_d = 2.75 \times 10^{-2} \times 10^{0.291M} \times 0.265$	0.61
	Soft All.	$T_d = 2.28 \times 10^{-1} \times 10^{0.199M} \times 0.233$	0.52
	Total	$T_d = 2.08 \times 10^{-2} \times 10^{0.274M} \times 0.394$	0.65
N_z	Rock	$N_z = 1.43 \times 10^{-2} \times 10^{0.410M} \times 0.444$	0.75
	Dil.	$N_z = 4.23 \times 10^{-1} \times 10^{0.0974M} \times 0.681$	0.66
	All.	$N_z = 6.28 \times 10^{-1} \times 10^{0.272M} \times 0.0313$	0.54
	Soft All.	$N_z = 4.05 \times 10^{0.190M} \times -0.0646$	0.29
	Total	$N_z = 4.68 \times 10^{-1} \times 10^{0.243M} \times 0.195$	0.54

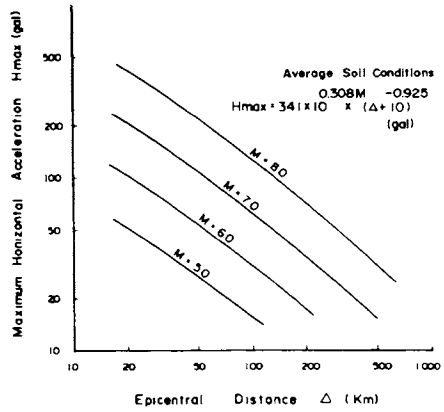

Fig. 3 Example of Epicentral Distance vs. Peak Horizontal Acceleration

As for the three remaining characteristic variables T_1, v, and T_m, the multiple correlation coefficients are found to be less than 0.5. This denotes that there is no distinct relation among these variables and M and Δ. For these variables the mean values and the standard deviations are evaluated depending on soil conditions, and are listed in Table V.

Table V Averages and Standard Deviations of T_1, v, and T_m

		Subsoil Condition: Rock	Diluvium	Alluvium	Soft Alluvium
T_1 (sec)	Average	0.36	0.43	0.49	0.75
	S.D.	0.52	0.39	0.30	0.42
$v = \frac{V_{max}}{H_{max}}$	Average	0.34	0.33	0.34	0.32
	S.D.	0.15	0.18	0.18	0.21
T_m (sec)	Average	0.30	0.34	0.39	0.61
	S.D.	0.36	0.22	0.22	0.35
T_1/T_m		1.20	1.26	1.26	1.23

Although it is obvious from the correlation of Table IV that the results will give only rough approximation, the analysis may provide a tendency of strong-motion properties, and can be summarized as follows :

(1) The peak horizontal acceleration (H_{max}), the duration of major motion (T_d), and the number of zero-crossing (N_Z) can be approximately expressed as functions of earthquake magnitude (M) and epicentral distance, for respective soil conditions.

(2) The duration of major motion (T_d) defined in Fig.2 gets longer as the earthquake magnitude becomes greater and as the epicentral distance becomes longer.

(3) The relation between the number of zero-crossing (N_Z) and the epicentral distance (Δ) is considerably affected by soil conditions. The value of N_Z increases with the increase in Δ for harder soils. It seems that N_Z is not affected by Δ but by M, for softer soils. The number of repetitions of major motions which can be approximately $N_Z/2$, is 30 to 100 for various soil conditions.

(4) The period of vibration (T_1) near the time of H_{max}, the ratio of vertical to horizontal accelerations (v), and the mean period of vibration (T_m) during the major motions are not clearly related with M or Δ. The following two points, however, can be seen.

  (a) The mean values of T_1 and T_d get longer as soils become softer. This tendency is obvious for soft alluvial deposits. The ratio of T_1 to T_d is 1.20 to 1.26, and the ratio is almost constant, irrespectively of soil conditions.

  (b) The mean value of v being 0.32 to 0.34 is not strongly affected by soil conditions. Since the standard deviation is 0.15 to 0.21, the vertical acceleration can generally assumed to be about one half of the horizontal acceleration.

Fig.4 illustrates the frequency characteristics of the most typical SMAC-B2 accelerograph used in the free-field strong-motion measurements in Japan. Since in the above analysis no correction was made with respect to frequency characteristics, it should be noted that acceleration with high frequency components are significantly suppressed.

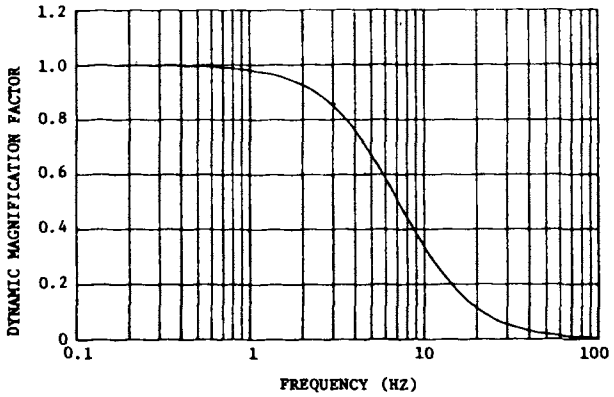

Fig. 4 Frequency Characteristics of SMAC-B2 Accelerograph

In this connection, Goto et al (1978) has attempted frequency correction of SMAC-B2 records, and obtained relationships between recorded peak acceleration and corrected peak acceleration for 70-component records triggered on free field grounds with various soil conditions. Table VI and Fig.5 give the typical results.

Table VI Effects of Soil Conditions on Correction of Accelerograms (Goto et al (1978))

Soil Condition	Number of Sites	Number of Records	Peak acceleration (gal) recorded	Peak acceleration (gal) corrected	Amplification* range	Amplification* mean
Type I	2	8	75 ~ 112	118 ~ 164	1.29 ~ 1.81	1.63
Type II	5	18	33 ~ 233	41 ~ 244	1.06 ~ 1.99	1.34
Type III	9	27	43 ~ 230	59 ~ 282	1.07 ~ 1.72	1.31
Type IV	7	17	64 ~ 230	70 ~ 266	0.91 ~ 1.36	1.10

*Amplification = corrected peak acceleration / recorded peak acceleration

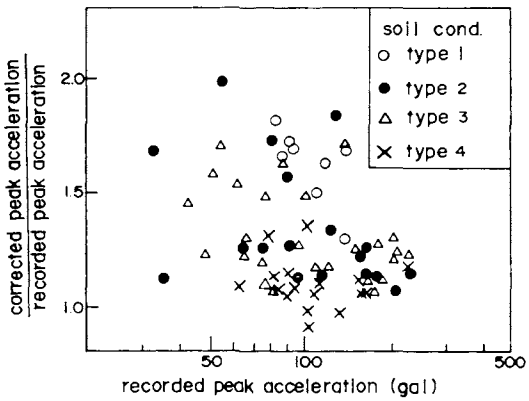

Fig. 5 Amplification of Peak Acceleration due to Correction (Goto et al (1978))

Crouse and Turner (1980) have recently performed similar studies for Japanese records obtained by SMAC-B2 accelerographs, and provided a result shown in Fig.6. These data indicate that the ratio of corrected peak ac-

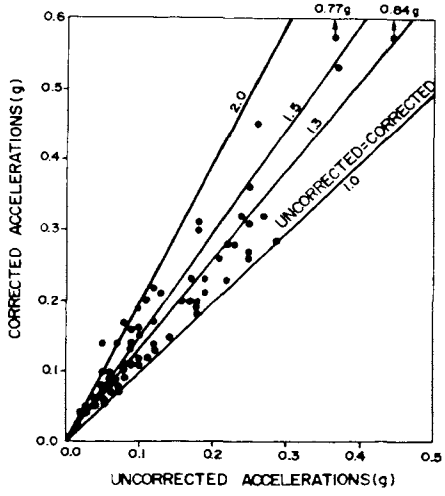

Fig. 6 Peak Accelerations for Uncorrected and Corrected Japanese Accelerograms (Crouse and Turner (1980))

celeration to recorded uncorrected peak acceleration is on the order of 0.9 to 2.0. The ratio will be higher for hard soils and get lower for soft soils. The results by Iwasaki et al (1978) should be re-examined in consideration of the effects of the correction.

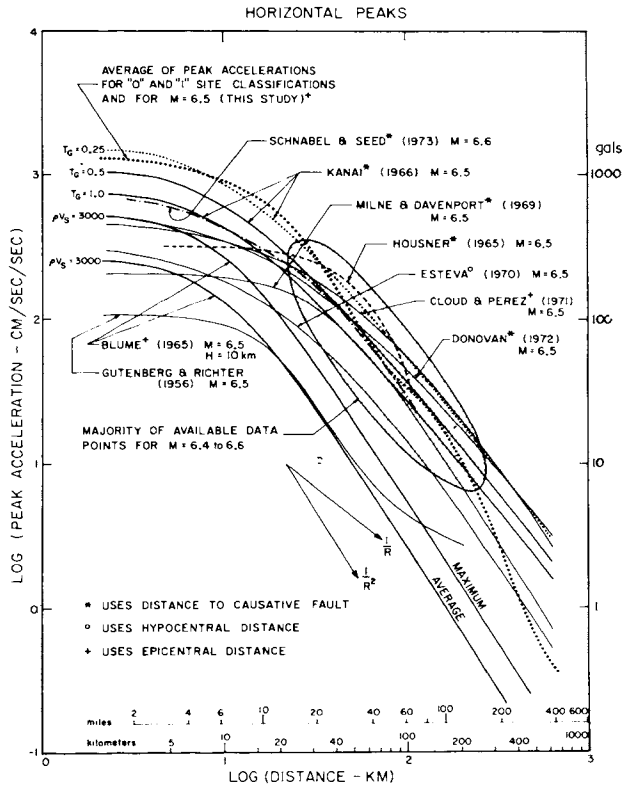

Fig. 7 Comparison of the Relation of Distance and Peak Acceleration for Magnitude 6.5 (Trifunac and Brady (1975))

For U.S. records there are a number of investigations on peak acceleration. Trifunac and Brady (1975) examined many of relations between distance and peak acceleration, and showed Fig.7 for an earthquake with magnitude 6.5.

Jennings and Helmberger (1978) presented Fig.8 which indicates plots of peak acceleration versus distance for

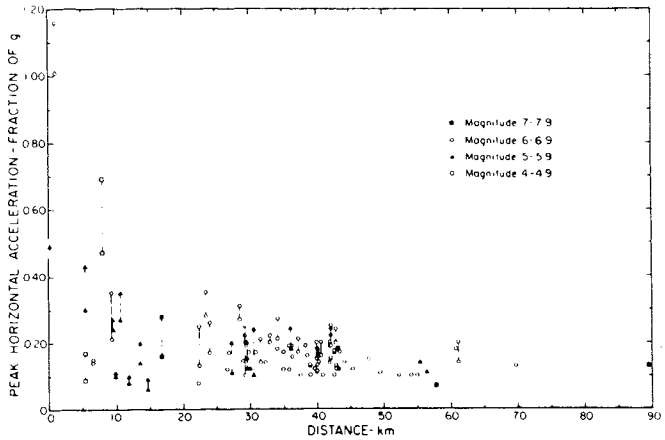

Fig. 8 Peak Acceleration vs. Distance for Four Magnitude Classes (Jennings and Helmberger (1978))

earthquakes with different magnitude levels. The figure illustrates variability of the data and suggests the difficulty in establishing simple relations among magnitude, distance and peak acceleration.

Idriss (1978) also discussed a number of different studies of distance-magnitude-acceleration relations and found that there is not yet a consensus among the many studies.

ANALYSES OF RESPONSE SPECTRA

Outlines of Response Spectrum Analysis

The response spectrum technique is now widely used for the dynamic analysis of structures subjected to earthquake excitation (Katayama et al (1977)). Earthquake response spectra of strong-motion records account for two principal features, i.e., frequency characteristics and intensities of ground shaking on structures. The former is characterized by the spectral shape, whereas the latter by the spectral amplitude. A design response spectrum can be obtained from a number of spectra computed from actual strong-motion records usually through normalization and averaging. Normalization is performed in order to extract the frequency characteristics alone. In Japan, acceleration response spectra are commonly normalized by the peak acceleration of the record. Normalized response spectra are often classified into several groups according to recording-site soil conditions. They are then averaged and smoothed to obtain design acceleration magnification spectra.

Although such a design spectrum is doubtlessly an efficient and practical engineering tool for the earthquake-resistant design of structures, it should be pointed out that some of the important properties contained in each original response spectrum are lost through the process of normalization and averaging. It is well recognized that spectral shape is influenced by earthquake magnitude and source-to-site distance. Most of the conventional design spectra, however, do not explicitly take account of these effects.

The results of statistical analysis of absolute response acceleration spectra of 277 horizontal components of strong-motion records obtained in Japan are shown in the following sections (Katayama et al (1977)). The method of statistical analysis adopted here is different from those used by previous investigators (McGuire (1974), Trifunac (1977)). Earthquake magnitude, epicentral distance, and recording-site soil conditions are chosen as three principal parameters. No functional relationship was assumed between the spectral amplitude and these parameters. Prediction of an average acceleration spectral amplitude may be performed by simply calculating a product of three factors, and the average spectrum may be modified to obtain the spectrum with a specified probability of being exceeded through an additional multiplication.

Strong-Motion Records Analyzed

In the analysis only free-field accelerograms recorded at stations on ground surface were used. Any records on structures (including the first floor and basement) are

excluded. A total of 277 horizontal components of accelerograms obtained in 19 years between 1956 and 1974 during 67 earthquakes were used. Fig.9 shows the distribution of magnitudes for the 67 earthquakes. Earthquakes with magnitudes less than 4.5 or with focal depth greater than 60 km were excluded in the data. About three quarters of the earthquakes have magnitudes between 5 and 7. Only four earthquakes with magnitude of 7.5 or greater, which include the Niigata Earthquake of 1964 (M=7.5) and the Tokachi-oki Earthquake of 1968 (M=7.9), were analyzed. Fig.10 indicates the distribution of peak accelerations of the 277-component records. It is seen that about 80 % of the data correspond to accelerograms with peak acceleration less than 100 gals.

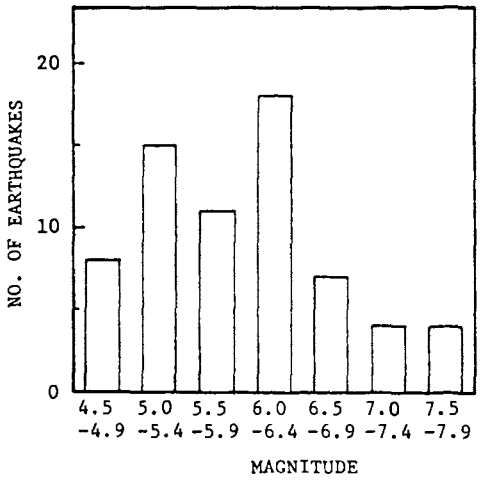

Fig. 9 Histogram of Magnitudes of 67 Earthquakes Used for Analysis (Katayama et al (1977))

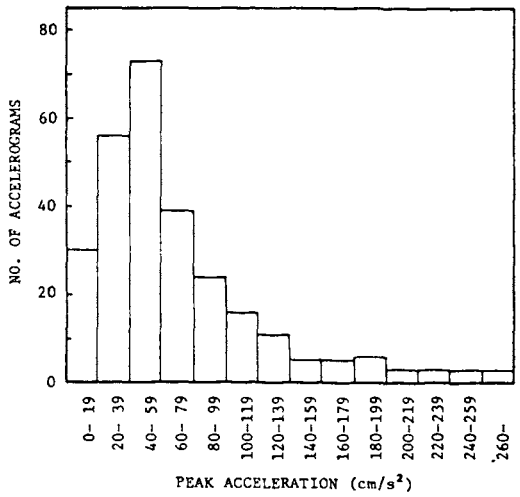

Fig. 10 Histogram of Peak Acceleration of 277 Accelerograms Used for Analysis (Katayama et al (1977))

The absolute acceleration response spectrum curve was represented by spectral amplitudes at 18 discrete natural periods as follows :

$$T = 0.1,\ 0.15,\ 0.2,\ 0.25,\ 0.3,\ 0.35,\ 0.4,\ 0.5,\ 0.6,\ 0.7,\ 0.8,\ 0.9,\ 1.0,\ 1.5,\ 2.0,\ 2.5,\ 3.0,\ \text{and } 4.0 \text{ (sec)} \quad (2)$$

The damping ratio of the single-degree-of-freedom (SDOF) system was assumed to be 5 % of critical.

Method of Analysis

Assume a set of N observed values and let the i-th value be denoted by A_i. Each item is then divided into several categories.

Define a variable x_{ijk} corresponding to category k in item j of sample i so that this variable takes a value of one if the properties of sample i react to category k in item j, and zero otherwise. Strictly speaking, k should be k_j, but suffix j is dropped for simplicity. Denote the unknown category value for category k in item j by w_{jk} and consider a quantity

$$\alpha_i = \sum_{j=1}^{R} \sum_{k=1}^{K_j} x_{ijk}\, w_{jk} \quad (3)$$

in which Kj is the number of categories in item j. The number of unknown category value is given by

$$\sum_{j=1}^{R} K_j \quad (4)$$

and w_{jk}'s are determined in such a way that the N observed values A_i best agreement is to minimize the sum of the squares of the difference between observed and predicted values:

$$\sum_{i=1}^{N} (A_i - \alpha_i)^2 \longrightarrow \text{Minimum} \quad (5)$$

Once the optimum w_{jk}'s are determined, the correlation coefficient

$$r = \frac{\frac{1}{N}\sum A_i \alpha_i - \bar{A}\bar{\alpha}}{\sigma_A \cdot \sigma_\alpha} \quad (6)$$

indicates whether or not the actual phenomenon is satisfactorily expressed by the statistical model. In eq. (6), $\bar{A}$ and $\bar{\alpha}$ are the means, and σ_A and σ_α are the standard deviations of A_i and α_i, respectively.

It is seen that eq. (3) assumes that a predicted value is obtained by the sum of relevant category values. If it is considered appropriate to assume that a predicted value be obtained by the product of category values, eq. (3) should be replaced by

$$\alpha_i = \prod_{j=1}^{R} \prod_{k=1}^{K_j} w_{jk}^{\,x_{ijk}} \quad (7)$$

By taking the logarithm of the both sides of eq. (7), the mathematical expression is reduced to

$$\log \alpha_i = \sum_{j=1}^{R} \sum_{k=1}^{K_j} x_{ijk}\, (\log w_{jk}) \quad (8)$$

which is essentially the same in form as eq. (3). The quantities $\bar{A}$, $\bar{\alpha}$, σ_A, and σ_α in eq. (6) are the means and the standard deviations of log A_i and log α_i, respectively.

Table VII Items and Categories Used for Quantification Analysis (Katayama et al (1977))

ITEM	CATEGORY	MEAN FOR THE DATA IN EACH CATEGORY
EARTHQUAKE MAGNITUDE (M)	M = 4.5 ~ 5.3	4.96
	M = 5.4 ~ 6.0	5.75
	M = 6.1 ~ 6.7	6.30
	M = 6.8 ~ 7.4	7.06
	M = 7.5 ~ 7.9	7.65
EPICENTRAL DISTANCE (Δ : km)	Δ = 6 ~ 19	11.7
	Δ = 20 ~ 59	38.2
	Δ = 60 ~ 119	82.9
	Δ = 120 ~ 199	158.7
	Δ = 200 ~ 405	271.3
GROUND CONDITION AT RECORDING SITE	TYPE I : TERTIARY OR OLDER ROCK (DEFINED AS BEDROCK), OR DILUVIUM WITH H* <10 m.	
	TYPE II : DILUVIUM WITH H > 10 m, OR ALLUVIUM WITH H <10 m.	
	TYPE III : ALLUVIUM WITH H < 25 m INCLUDING SOFT LAYER** WITH THICKNESS LESS THAN 5 m.	
	TYPE IV : OTHER THAN THE ABOVE, USUALLY SOFT ALLUVIUM OR RECLAIMED LAND.	

* DEPTH TO BEDROCK.

** SAND LAYER VULNERABLE TO LIQUEFACTION OR EXTREMELY SOFT COHESIVE SOIL LAYER.

Application to Spectral Amplitude Data

Statistical analysis was performed for the 277 acceleration spectral amplitudes (damping ratio of 5 % of critical) at the 18 natural periods shown in eq. (2) by using the method described in the preceding section. Three items, i.e., earthquake magnitude, epicentral distance, and soil conditions, were selected in the analysis.

The items and categories used in the analysis are listed in Table VII. It is noted that magnitude and epicentral distance, which are continuous quantities in nature, are also divided into several discrete categories. By using these categories in the method previously mentioned, no functional relationship need be assumed between the spectral amplitude and the relevant parameters.

Table VIII shows the distribution of the number of the data set in each of the combinations of items and categories. As seen from the table, the data used are far from sufficient in number nor uniform in distribution. Data of large magnitude earthquake with short epicentral distance are quite few.

In view of the preliminary analysis, the prediction formula in this analysis was taken in the following form:

$$\bar{S}_A(T, h) \quad f_M(T, h) \times f_\Delta(T, h) \times f_s(T, h) \qquad (9)$$

where

$\bar{S}_A(T, h)$ = Predicted absolute acceleration response of a SDOF system with given T and h (gals),

T = Natural period of SDOF system (sec),

h = Damping ratio of SDOF system = 0.05,

$f_M(T, h)$ = Weighting factor for each magnitude category in Table VII,

$f_\Delta(T, h)$ = Weighting factor for each distance category in Table VII

$f_s(T, h)$ = Weighting factor for each soil category in Table VII.

Table VIII Distribution of Data Set Used for Quantification Analysis (Katayama et al (1977))

MAGNITUDE M	GROUND CONDITION	EPICENTRAL DISTANCE Δ(km) 6~19	20~59	60~119	120~199	200~405	TOTAL	
4.5 ~ 5.3	TYPE I	6	4				10	60
	TYPE II	4	10				14	
	TYPE III	12	8	8	2		30	
	TYPE IV	6					6	
5.4 ~ 6.0	TYPE I		4	2			6	48
	TYPE II	4	4	4			12	
	TYPE III	2	12	6			20	
	TYPE IV	4	2	4			10	
6.1 ~ 6.7	TYPE I		4	6			10	102
	TYPE II		4	4	2		10	
	TYPE III	4	32	22	8	2	68	
	TYPE IV		6	4	2	2	14	
6.8 ~ 7.4	TYPE I			4	3	2	9	29
	TYPE II			2	4	2	8	
	TYPE III				4	4	8	
	TYPE IV					4	4	
7.5 ~ 7.9	TYPE I				2	2	4	38
	TYPE II				6	2	8	
	TYPE III		2	6	4	2	14	
	TYPE IV				2	10	12	
TOTAL		42	92	72	39	32	277	

The values of weighting factors determined from the statistical analysis are shown in Table IX, for each of the 18 periods in eq. (2). For example, the absolute acceleration response spectral amplitude for T=0.5 sec and h = 0.05 that would be obtained from the ground motions caused by an earthquake with M=6.1 ~ 6.7, and Δ =20 ~ 59 km, and recorded on the surface of Type III soil, is predicted by eq. (9) and Table IX as follows:

$$\bar{S}_A(0.5, 0.05) = 0.309 \times 2.91 \times 140 = 126 \text{ (gals)}$$

Examples of predicted response spectra are shown in Fig. 11.

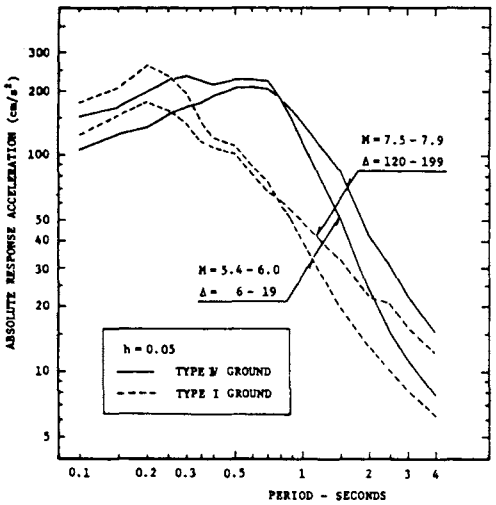

Fig. 11 Example of Predicted Acceleration Spectra (Katayama et al (1977))

Table IX Weighting Factors Obtained from Quantification Analysis (Katayama et al (1977))

T	r	f_M (T, 0.05) MAGNITUDE (M)					f_Δ (T, 0.05) EPICENTRAL DISTANCE (Δ : km)					fs (T, 0.05) SOIL CONDITION (S)			
		4.5~5.3	5.4~6.0	6.1~6.7	6.8~7.4	7.5~7.9	6 ~19	20~59	60~119	120~199	200~405	TYPE I	TYPE II	TYPE III	TYPE IV
0.10	0.56	0.218	0.278	0.296	0.399	1.00	5.10	2.67	2.05	0.994	1.00	126	107	120	106
0.15	0.53	0.225	0.274	0.297	0.448	1.00	4.85	3.01	2.15	1.00	1.00	155	130	141	125
0.20	0.54	0.185	0.280	0.288	0.499	1.00	5.48	3.24	2.07	1.05	1.00	169	149	161	129
0.25	0.55	0.171	0.254	0.283	0.534	1.00	6.86	3.65	2.33	1.21	1.00	135	129	143	129
0.30	0.56	0.164	0.269	0.280	0.548	1.00	6.59	3.51	2.25	1.27	1.00	109	130	147	131
0.35	0.55	0.161	0.274	0.302	0.588	1.00	5.74	3.05	2.13	1.24	1.00	92.8	126	149	142
0.40	0.57	0.152	0.268	0.311	0.557	1.00	5.45	3.01	1.92	1.33	1.00	83.0	122	145	144
0.50	0.63	0.108	0.237	0.309	0.593	1.00	6.35	2.91	1.60	1.36	1.00	76.6	113	140	156
0.60	0.67	0.0889	0.246	0.321	0.618	1.00	5.88	2.79	1.46	1.32	1.00	62.1	101	134	159
0.70	0.70	0.0730	0.222	0.315	0.644	1.00	6.77	2.96	1.56	1.37	1.00	50.0	88.8	118	148
0.80	0.68	0.0683	0.214	0.294	0.595	1.00	5.89	2.73	1.54	1.28	1.00	47.9	91.0	115	145
0.90	0.67	0.0672	0.214	0.285	0.581	1.00	5.13	2.38	1.48	1.20	1.00	46.4	90.5	113	136
1.00	0.67	0.0653	0.204	0.284	0.636	1.00	4.62	2.15	1.40	1.16	1.00	43.3	89.3	107	125
1.50	0.72	0.0503	0.138	0.204	0.534	1.00	4.40	2.20	1.44	1.00	1.00	33.0	56.5	68.5	84.6
2.00	0.71	0.0605	0.148	0.215	0.585	1.00	3.66	1.99	1.29	0.924	1.00	24.7	36.8	44.1	46.2
2.50	0.70	0.0587	0.136	0.183	0.405	1.00	3.50	1.95	1.34	0.947	1.00	21.9	32.7	35.8	33.0
3.00	0.69	0.0660	0.138	0.194	0.391	1.00	3.26	1.79	1.35	0.867	1.00	18.8	26.6	28.5	26.6
4.00	0.68	0.0704	0.144	0.187	0.395	1.00	2.81	1.61	1.27	0.788	1.00	15.7	20.3	24.1	19.1

T = PERIOD (SECONDS), r = CORRELATION COEFFICIENT

The second column of Table IX shows correlation coefficients between observed and predicted spectral amplitudes for each natural period. Correlation is rather low, especially for short periods. This indicates that the deviations of observed values about the predicted value should be carefully investigated. This problem will be discussed in one of the succeeding sections.

Characteristics of Predicted Spectra

The effects of earthquake magnitude on the absolute acceleration spectral amplitude for a fixed combination of distance and soil condition categories are shown in Fig.12. The effects are illustrated in terms of the weighting factor of a certain magnitude category to that of the magnitude category of M=4.5~5.3. It is seen that the effects of magnitude are different for different period ranges of a SDOF system. The increase in magnitude from the smallest (M=4.5~5.3) to the largest category (M=7.5~7.9) investigated in this study causes about 5 to 6-fold increase in the response acceleration for natural periods shorter than about 0.4 sec, whereas the same increase in magnitude produces approximately 14 to 20-fold increase in the response acceleration for periods longer than about 0.7 sec. This clearly indicates that large earthquakes are characterized by greater contents of long-period waves, which is a trend repeatedly discussed by previous investigators. As far as Fig.12 is concerned, the effects of earthquake magnitude are most noticeable in the range of natural periods between about 0.7 and 2.5 sec.

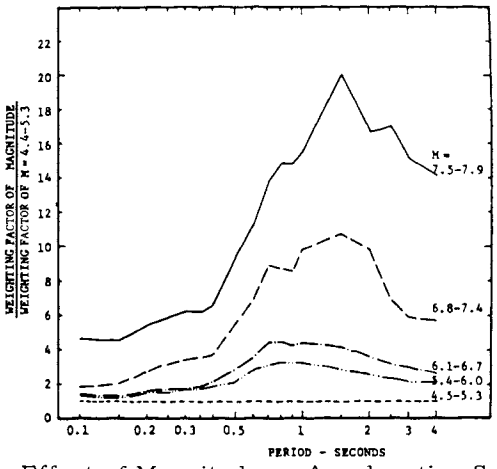

Fig. 12 Effect of Magnitude on Acceleration Spectra (Katayama et al (1977))

The effects of epicentral distance is illustrated in Fig. 13, in which are shown the ratios of weighting factors for different distance categories to that for Δ=200-405 km category. The increase in response accelerations

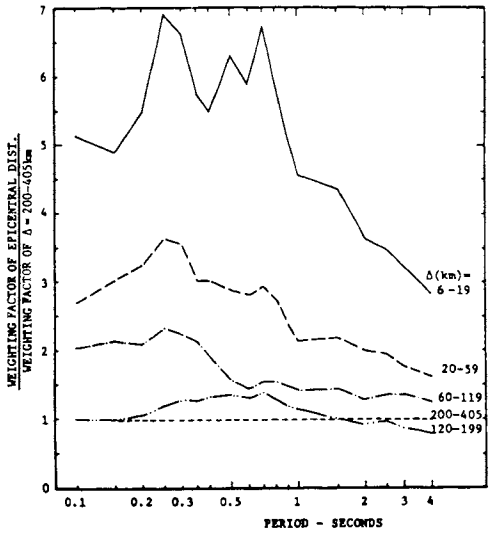

Fig. 13 Effects of Epicentral Distance on Acceleration Spectra (Katayama et al (1977))

due to the decrease in epicentral distance is seen to be more predominant for SDOF systems with natural periods shorter than about 0.8 sec. This substantiates a well-known property that the ground motions caused by near-field earthquakes strongly contain shorter-period components than those caused by distant earthquakes.

Fig. 14 shows the effects of recording-site soil conditions on the response spectra in terms of the ratios of weighting factors for different soil condition categories to that for Type I soil. It is interesting to note that the effects of soil conditions are very clearly illustrated. The effects are most noticeable in the period range of SDOF systems between 0.5 and 2.0 sec, in which absolute response accelerations increase as soils become softer.

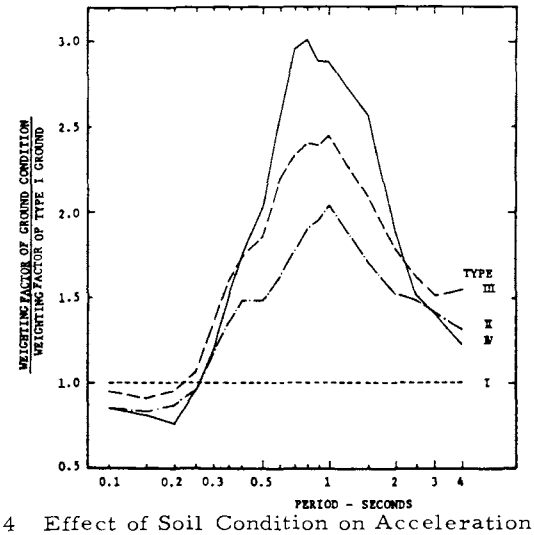

Fig. 14 Effect of Soil Condition on Acceleration Spectra (Katayama et al (1977))

Scatter of Observed Response about Prediction

As seen in Table IX, a correlation between predicted values $\bar{S}_A$ and observed values S_A may be regarded rather low. This indicates that observed spectra exhibit considerable deviations from the predicted spectra. For example, it is seen from Table VIII that there are 32-component accelerograms for the combination of M=6.1 ~ 6.7, Δ = 20~59 km, and Type III soil. Fig. 15 illustrates the predicted spectrum for this particular combination of categories and the ranges of observed spectra of the 32 components. Two principal reasons can be pointed out for such a large scatter: (1) The numbers of categories in the three items are small. Each magnitude and distance category includes a wide range of variation, and the soil condition categories are not very accurate. (2) Only three principal factors are selected for parameters that may influence response spectra, but there are many other parameters such as properties of source-to-site wave transmission paths, focal mechanisms, deeper site conditions, etc.

Let the ratio of an observed spectral amplitude S_A and the predicted amplitude $\bar{S}_A$ be denoted by α :

$$\alpha = S_A / \bar{S}_A \qquad (10)$$

There are 277 α-values available at each of the 18 periods shown in eq. (2). Figs. 16~19 show histograms

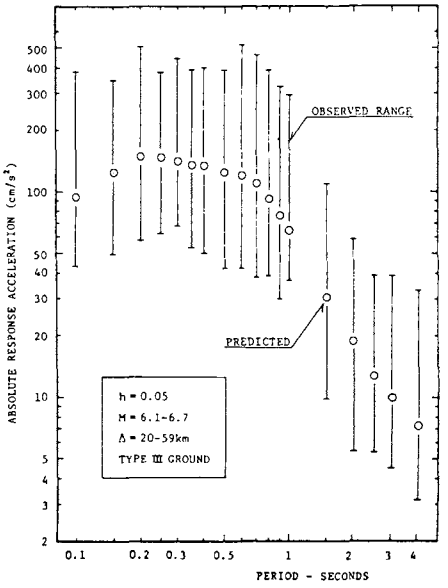

Fig. 15 Example of a Relation of Predicted Value and Observed Range of Acceleration Spectral Amplitude (Katayama et al (1977))

of these ratios at four selected natural periods of a SDOF system. All of these histograms have distributions considerably skewed to the right and apparently resemble the lognormal distribution. The means and standard deviations of α are listed in Table X. The χ^2-fit test was applied to the values of α by assuming the lognormal distribution with the parameters m_α and σ_α estimated from the data. The computed χ^2-values are also shown in Table X for the 18 periods. Since the number of intervals used for this analysis was 15, the number of degree of freedom becomes 12 and the critical value at the 5 % significant level is

$$\chi^2_{0.05,\ 12} = 21.03$$

The computed χ^2-values except for two cases (T=0.15 and 0.2 sec) are less than the critical. Therefore, it may be concluded that the data are not in significant contradiction to the lognormal model.

If α is assumed to be lognomally distributed, the value of α for a specified probability of being exceeded, p, can be easily evaluated. Such values of α for p=0.05, 0.1, 0.2, 0.3, 0.4 and 0.5 are also given in Table X. It is understood that the values of α for a given probability p are almost constant regardless of period T. Hence the averages shown in the bottom line of Table X may be regarded as the representative values. When the predicted spectrum amplitude $\bar{S}_A$ computed by eq. (9) and Table IX is combined with the factors given in Table X, an absolute acceleration response spectrum for a given probability of being exceeded can be obtained.

Comparison of Average Spectrum Curves between Japan and the Western United States

In the U.S., several statistical studies similar to the previous sections have been made using U.S. strong-motion data obtained in the western United States.

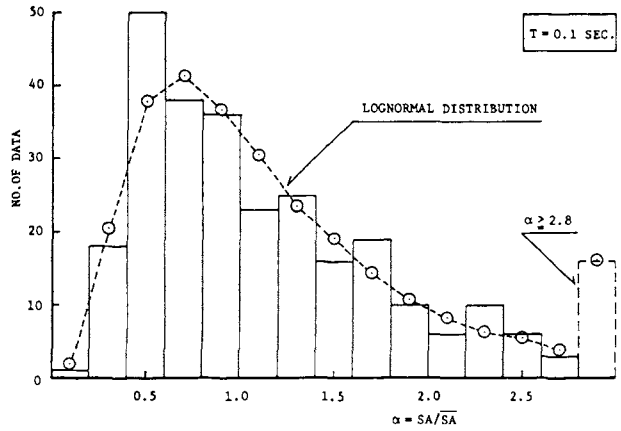

Fig. 16 Histogram of α for T = 0.1 sec

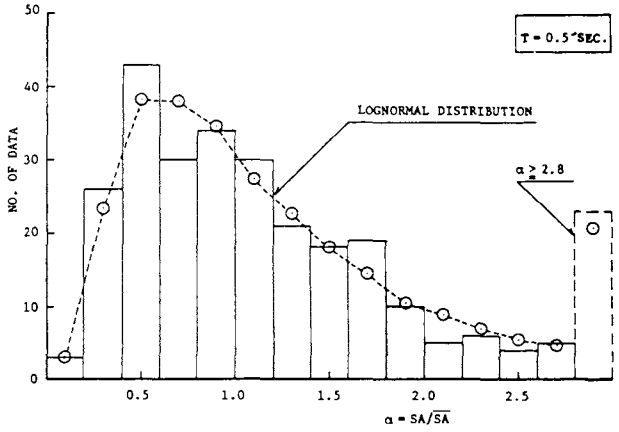

Fig. 17 Histogram of α for T = 0.5 sec

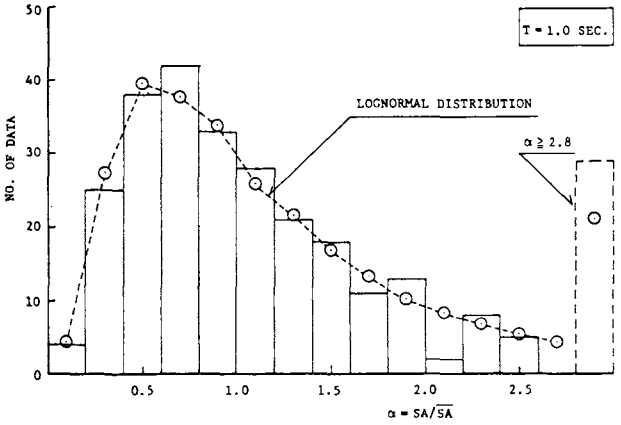

Fig. 18 Histogram of α for T = 1.0 sec

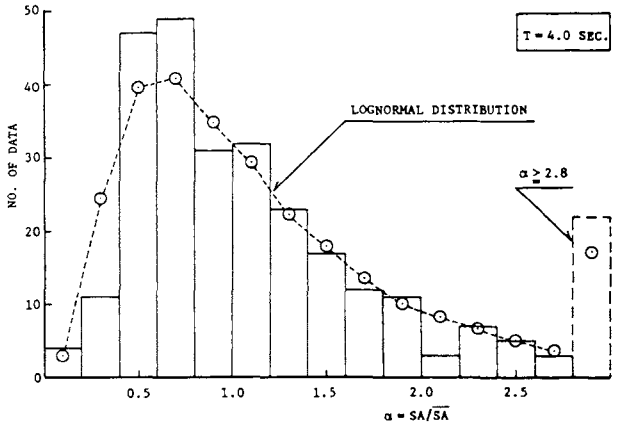

Fig. 19 Histogram of α for T = 4.0 sec

Table X Value of $\alpha = S_A/\bar{S}_A$ for Specified Probabilities of Being Exceeded (Katayama et al (1977))

(1)	(2)	(3)	(4)	(5)					
T (sec)	m_α	σ_α	χ^2	VALUE OF α CORRESPONDING TO p.					
				p=0.05	p=0.1	p=0.2	p=0.3	p=0.4	p=0.5
0.1	1.24	0.910	11.78	2.94	2.32	1.75	1.41	1.18	1.00
0.15	1.25	0.882	31.66	2.90	2.31	1.74	1.42	1.20	1.02
0.2	1.27	0.914	26.34	2.98	2.36	1.77	1.44	1.21	1.03
0.25	1.26	0.968	19.78	3.06	2.39	1.77	1.43	1.19	1.00
0.3	1.26	0.948	10.19	3.04	2.38	1.78	1.43	1.20	1.01
0.35	1.29	1.10	9.10	3.31	2.53	1.83	1.45	1.18	0.98
0.4	1.26	0.999	11.50	3.12	2.42	1.78	1.42	1.18	0.99
0.5	1.30	1.05	6.93	3.24	2.51	1.84	1.46	1.21	1.01
0.6	1.29	1.11	10.40	3.33	2.54	1.83	1.44	1.18	0.98
0.7	1.34	1.32	16.80	3.70	2.74	1.91	1.47	1.18	0.96
0.8*	1.27	1.02	9.56	3.16	2.45	1.79	1.43	1.18	0.99
0.9*	1.29	1.08	12.55	3.28	2.52	1.83	1.45	1.19	0.99
1.0*	1.28	1.09	14.47	3.28	2.51	1.81	1.43	1.17	0.97
1.5*	1.23	1.00	17.01	3.08	2.38	1.74	1.39	1.14	0.95
2.0*	1.23	0.956	7.37	3.01	2.35	1.73	1.39	1.16	0.97
2.5*	1.27	1.14	14.97	3.34	2.53	1.80	1.41	1.15	0.95
3.0*	1.24	1.01	19.45	3.11	2.40	1.75	1.40	1.15	0.96
4.0*	1.23	0.953	16.49	3.00	2.34	1.73	1.39	1.16	0.97
AVERAGE				3.16	2.44	1.79	1.43	1.18	0.99

(1) T = Period (sec)
(2) m_α = Mean of α
(3) σ_α = Standard deviation of α
(4) $\chi^2 = \sum_{i=1}^{n} \frac{(Fi-fi)^2}{Fi}$: $\chi^2_{0.05,12} = 21.03$
Fi = Expected number of occurrences
fi = Observed number of occurrences
(5) p = Probability of being exceeded
* Two data out of 277 omitted for calculation of m_α, σ_α

Crouse and Turner (1980) have studied response spectrum curves of Japanese SMAC-B2 accelerograms using the standard U.S. data processing method. Fig. 20 indicates a comparison of response spectra (pseudovelocity) of uncorrected and corrected accelerograms of a Japanese record. It is seen from the study that the corrected spectrum does not differ significantly from the uncorrected one except for records having relatively high frequency components. Since the general attention of a structural design is paid to the intermediate portion of the frequency spectra, a comparison study of rosponse spectrum characteristics can be made with a sufficient accuracy between the Japanese and the U.S. records.

Hudson (1980) has attempted to compare the Japanese average spectrum curves described in the previous sections with U.S. ones proposed by Trifunac and Anderson (1977). Fig.21 shows the comparison between the Japanese curves and the U.S. ones. The solid curves without data points are derived from the smoothed curves of Trifunac and Anderson for the U.S. data. The solid curves with circular data points are the average curve plotted directed from Table IX. This comparison is for a magnitude 6.4 earthquake occurring at a distance of 40 km.

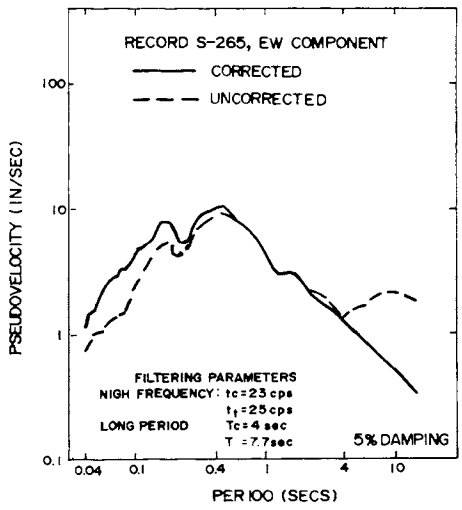

Fig. 20 Example of Response Spectra of Uncorrected and Corrected Accelerogram of SMAC-B2 (Crouse and Turner (1980))

From Fig.21, Hudson (1980) indicates that there are several remarkable similarities between the two data sets, and also some significant differences. The overall shape of the average response spectrum curves is much the same, and in both cases a hard site responds more than a soft site at low periods, and less at high periods. The cross-over period for the hard and soft spectrum curves occurs at practically the same period of 0.25 sec for the both data sets. The main difference is the lower level of the Japanese average curves, which are smaller by factors of 2 to 3.

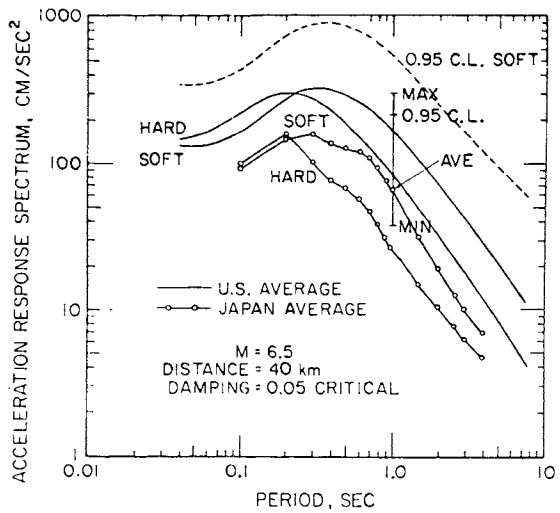

Fig. 21 Average Acceleration Response Spectrum Amplitudes for U.S. and Japanese Earthquakes (Hudson (1980))

The apparent lower level of the Japanese average spectrum curves may be explained by systematic differences in magnitude determinations, in natures of focal mechanisms and focal depths, in definitions of distance, or in distance attenuation relationships.

DENSE INSTRUMENT ARRAY PROGRAMS FOR OBSERVATION OF STRONG-MOTION EARTHQUAKES

Outline

From the knowledges accumulated through past strong-motion observations, it is widely recognized that characteristics of ground motion differ site by site, and that characteristics of ground motions with short to medium period range are significantly dependent on seismic source mechanisms, wave transmission paths from the source area to the observation station, and local geological and topographical conditions near the station. Recently it is also recognized that, in order to investigate the abovementioned effects, observations through dense instrument arrays deployed concentratedly and systematically in some specific areas, are indispensable together with the conventional strong-motion observations.

With consideration of the above situations, it was decided to hold an International Workshop on Strong-Motion Earthquake Instrument Arrays at the Executive Committee Meeting of the International Association for Earthquake Engineering held at New Delhi in January, 1977 at the occasion of the Sixth World Conference on Earthquake Engineering. The determination was supported firmly by the International Association of Seismology and Physics of the Earth's Interior.

The International Workshop was held at Honolulu, Hawaii in May, 1978 with participants from sixteen countries in the world, and adopted recommendations to establish an International Strong Motion Arrays Council for facilitating and collaborating the implementation of observation using dense strong-motion instrument arrays (Iwan (1978)). Basing upon a careful examination on potentials of occurrence of large earthquakes within coming ten years, twenty eight locations were selected for favorable array locations. Out of the twenty eight locations selected, six were assigned as high priority locations. Among these twenty eight locations, three were selected from Japan, namely, Eastern Tohoku, Suruga Bay-Izu and Southern Kanto, and Western Chubu. Furthermore, Suruga Bay-Izu and Southern Kanto area was designated as one of the high priority locations.

The Workshop also recommended typical array configurations depending on the causative fault models such as strike-slip fault, dip-slip fault and subduction-thrust fault for the analysis of source mechanism and wave path effects, together with configurations for the analysis of local effects such as local geological and topographical conditions. Mobil strong-motion instrument arrays for deploying immediately after either an announcement of earthquake prediction warning or an occurrence of a strong earthquake, were also recommended.

Prior to the International Workshop, a Working Group on Strong-Motion Earthquake Instrument Array was organized under the Liaison Committee of Earthquake Engineering, Japan Science Council in Japan. This Working Group has been serving as a national center for dense strong-motion instrument arrays observation with the function of coordinating and promoting the program of dense arrays observation. The program consists of three items : (1) Development of strong-motion earthquake instrument arrays system, (2) Deployment of

arrays for analyses of source mechanisms and wave paths effects, and (3) Deployment of arrays for local effects studies. In May, 1979, Japan Science Council made recommendations to the Prime Minister of the Japanese Government to enthusiastically promote the implementation of dense strong-motion instrument arrays programs. In the following sections recent topics on dense strongmotion instrument array programs and some observation results will be described.

Observation of Earthquake Response of Ground with Horizontal and Vertical Accelerometer Arrays at Haneda

Tsuchida et al (1977) and (1980) established a horizontal and two vertical accelerometer arrays for simultaneously recording ground motions at eight points distributed in a vertical plane in a soft ground. The observation started in 1974 at the Tokyo International Airport at Haneda, Tokyo. The location of array deployment site is shown in Fig. 22. In the figure D.H.A. denotes the direction of the horizontal array line. Detailed configurations of the installation are shown in Figs. 23 and 24. The soil profile beneath the array site is shown in Fig. 24.

The distance between ajacent surface observation points is 500 meters, and the total length of observation line is 2500 meters. Each point is equipped with transducers to

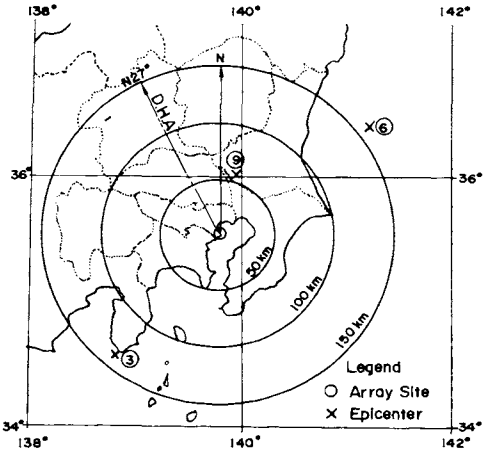

Fig. 22 Locations of Array Deployment Site and Epicenters of Three Earthquakes (Tsuchida et al (1978))

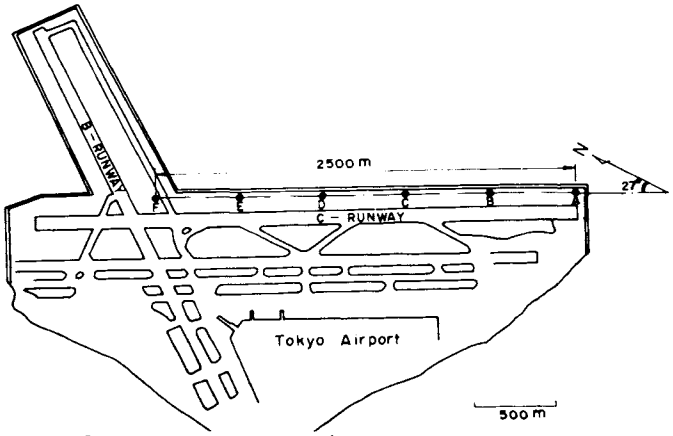

Fig. 23 Deployment of Accelerometers in Plan (Tsuchida et al (1978))

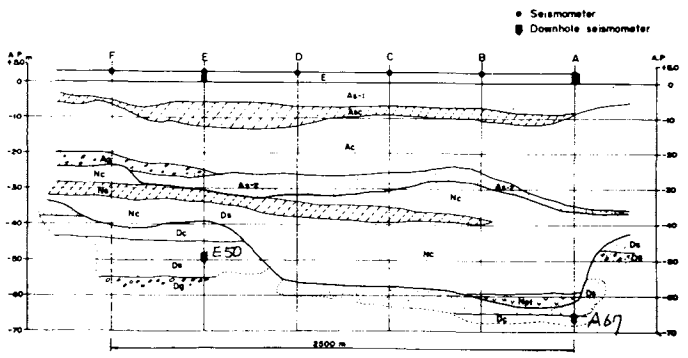

Key (Fill) E: Fill, (Alluvial deposit) A_{s-1}:Sand, A_{sc}:Silty sand, A_c: Silty clay, A_{s-2}: Sand, A_g: Sandy gravel, (Diluvial deposit) N_c: Silty clay, N_s: Silty sand, N_{pt}: Peat, D_s: Sand, D_g: Sandy gravel, D_c: Silt.

Fig. 24 Deployment of Accelerometers in Vertical Section and Soil Profile (Tsuchida et al (1978))

observe longitudinal and transverse components of ground accelerations. At the points A and E, the vertical accelerometer arrays are also established; the deeper accelerometers are at depths of 67.2 meters and 49.6 meters below the ground surface, respectively. The downhole accelerometers have three transducers to observe longitudinal, transverse, and vertical components of ground accelerations.

All the accelerometers are of moving coil type and outputs from them are recorded with four sets of electromagnetic oscillographs. Frequency range of the accelerometers for sensitivity decrement within 10 % is 0.1 to 35 Hz for the accelerometers on the ground surface and 0.5 to 50 Hz for the downhole accelerometers. The oscillograms are digitized for analysis with a computer on-line digitizer at an equal time interval of 0.01 sec.

Parameters of three earthquakes, named as TIA-3, TIA-6, and TIA-9, during which the accelerometers triggered important records, are listed in Table XI, together with maximum accelerations, maximum displacements, etc. The locations of the epicenters are shown in Fig.22. As an example, acceleration records of earthquake TIA-3 at the observation points A and E are shown in Fig.25. The figure compares acceleration histories at the ground surfaces and the downhole accelerometer locations.

Calculated displacements for the earthquake TIA-3 are shown in Fig.26. It is seen from the figure that the displacement histories at all the observation points are very similar each other. The maximum ground displacements calculated for the three earthquakes are listed in Table XI. From the ground displacement time histories, relative displacements between two adjacent points were calculated, and the maximum values of the relative displacements are also shown in Table XI.

The cross correlation functions between the time histories of the ground displacements at the points were calculated, and the time-shift for the maximum correlation between the points A and F were obtained as 0.19, 0.17, and 0.44 sec for the earthquakes TIA-3, 6, and 9, respectively. These are averages of the time-shifts of

Table XI Parameters of Three Earthquakes and Maximum Amplitudes of Accelerations, Displacements, and Stresses (Tsuchida et al (1977))

Record designation	TIA-3		TIA-6		TIA-9	
Date Time	May 9, 1974 08:33		July 8, 1974 14:15		August 4, 1974 03:17	
Hypocenter Latitude Longitude	 33.6°N 138.8°E		 36.4°N 141.2°E		 36.0°N 139.9°E	
Depth	10 km		40 km		50 km	
Magnitude	6.9		6.3		5.8	
Epicentral distance	140 km		161 km		54 km	
(Component)	Long.	Tran.	Long.	Tran.	Long.	Tran.
Maximum acceleration in gals						
Point A	15.0	9.1	6.4	6.1	20.0	24.6
B	14.0	9.8	11.4	8.8	47.0	35.8
C	16.3	12.8	9.6	7.5	36.6	31.0
D	21.7	11.2	11.7	9.1	29.3	22.5
E	23.2	19.2	10.7	11.4	51.8	32.4
F	18.5	13.0	11.7	11.9	40.9	34.7
A (-67.2m)	5.8	4.3	3.8	3.0	10.1	8.4
E (-49.6m)	10.1	5.6	5.5	4.4	23.1	13.8
Maximum displacement in cm (calculated)						
Point A	1.34	0.91	0.52	0.63	0.40	0.38
B	1.48	0.76	0.50	0.63	0.42	0.87
C	1.83	0.85	0.54	0.69	0.63	0.52
D	2.14	0.81	0.81	0.79	0.46	0.39
E	1.96	1.36	0.49	0.83	0.46	0.58
F	1.92	0.94	0.51	0.66	0.58	0.55
A (-67.2m)	0.72	0.51	0.37	0.25	0.16	0.18
E (-49.6m)	1.48	0.64	0.42	0.57	0.30	0.25
Maximum relative displacement in cm (calculated)						
Point A & B	0.50	0.59	0.16	0.16	0.39	0.31
B & C	0.37	0.64	0.19	0.13	0.22	0.87
C & D	0.71	0.61	0.13	0.25	0.51	0.34
D & E	0.74	0.53	0.32	0.21	0.34	0.27
E & F	0.64	0.64	0.68	0.24	0.23	0.26
Maximum stresses in a buried pipe (Dia. 1000 mm) in kg/cm^2 (calculated)						
Stress due to axial deformation	31		29		21	
Stress due to bending deformation	0.06		0.02		0.07	

longitudinal and transverse components. The difference of the time-shifts between both components were less than 0.03 sec, as far as the three earthquake records are concerned.

If it is assumed that the waves propagate from the epicenters straightly along the ground surface, the velocities of the wave propagation are evaluated to be 5.3, 2.6, and 4.4 km/sec for the earthquakes TIA-3, 6, and 9, respectively.

It was considered that a pipeline had existed at shallow depth in the ground along the observation line, and the dynamic stresses induced in the pipe due to the earthquake ground motions were computed. In the estimation a steel pipe of diameter of 1000 mm was assumed, and the rigidity was assumed to be neglected. Table XI indicates thus calculated stresses due to the longitudinal deformation of the pipe and stresses due to the horizontal bending deformations. These are the maximum values along the observation line. It is seen that the stresses due to bending deformations are considerably smaller than those due to longitudinal deformations.

Next, for investigating correlation of earthquake ground motions between two points, frequency response function (FRF) was calculated, considering the recorded ground motions at one point as an input and those at another point as an output. In calculating FRF, a smoothing window was used, of which equivalent window width was 0.2 Hz. If the seismic waves propagate straightly in a ground

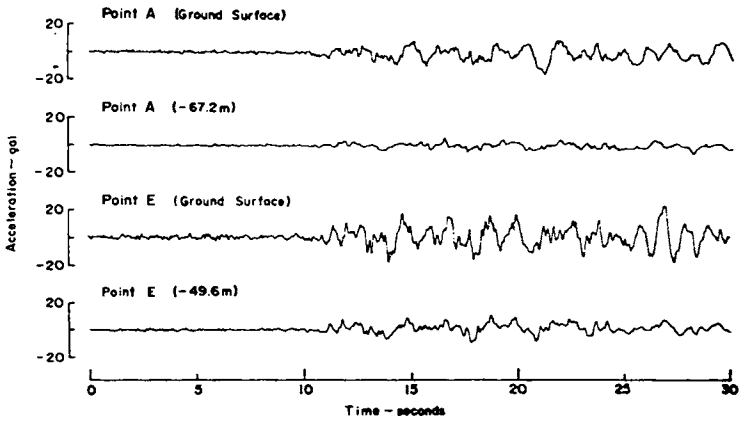

Fig. 25 Observed Ground Accerations (TIA-3, Longitudinal Component) (Tsuchida et al (1977))

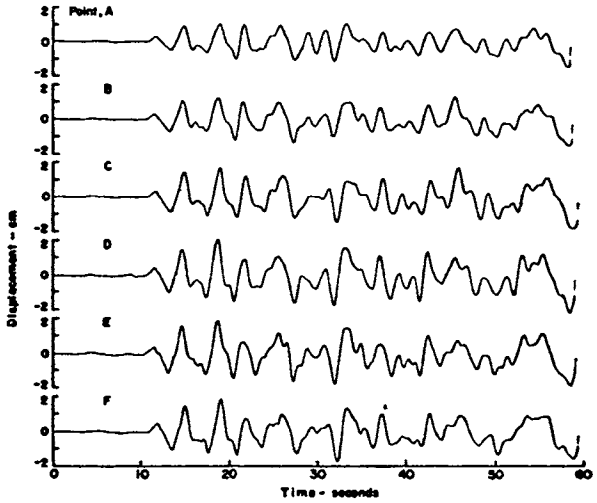

Fig. 26 Calculated Ground Displacements (TIA-3, Longitudinal Component) (Tsuchida et al (1977))

and no deformations of wave forms take place during the propagation, amplification of FRF is unity regardless of frequency. Several combinations of the points were selected and each FRF was calculated.

For making easier comparison of FRF for different components and different earthquakes, FRF of three earthquakes are plotted together in one figure. Beside, FRF of two horizontal ground motions are presented in one figure, and three FRF of the vertical ground motions are presented together.

Amplifications of FRF between the points A and B, B and C, and A and F are shown in Figs. 27 to 29. It is noticed that amplifications change as the frequency changes. This will deny a concept that seismic waves propagate

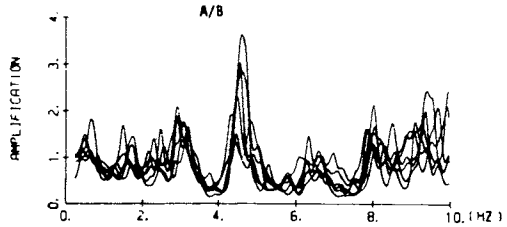

Fig. 27 FRF (Amplification) of A to B (Tsuchida et al (1978))

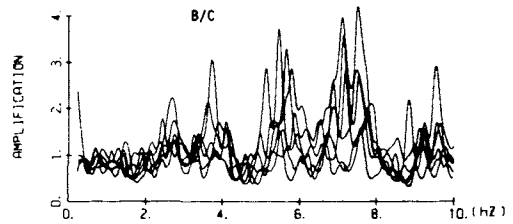

Fig. 28 FRF (Amplification) of B to C (Tsuchida et al (1978))

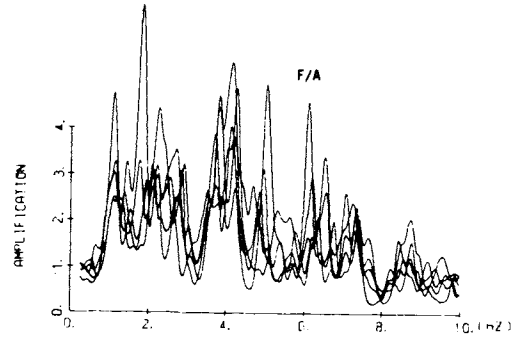

Fig. 29 FRF (Amplification) of F to A (Tsuchida et al (1978))

straightly in a constant amplitude along the ground surface. However, the six FRF of each combination of the points show very similar shapes.

Amplifications of FRF between the points A and A67, and between the points E and E50 are shown in Figs. 30 to 33. It is clear that FRF of the horizontal ground motions for the three earthquakes are very similar. FRF of the vertical ground motions of the three earthquakes have similar tendencies. However, there is no sharp peaks for the vertical.

FRF between the points A67 and E50 are shown in Figs. 34 and 35. Amplifications of FRF of the horizontal ground motions are not unity nor constant. The six amplification curves, however, are similar to each other in the frequency range lower than 6 Hz.

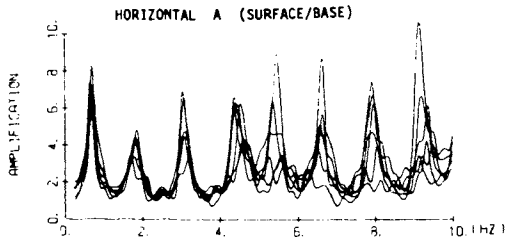

Fig. 30 FRF (Amplification) of A to A67 in Horizontal (Tsuchida et al (1978))

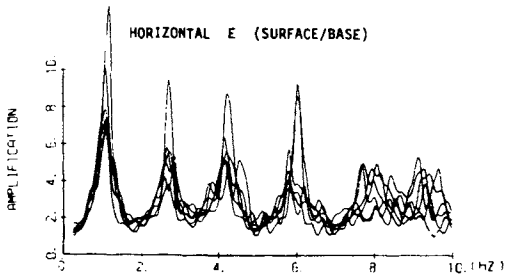

Fig. 31 FRF (Amplification) of E to E50 in Horizontal (Tsuchida et al (1978))

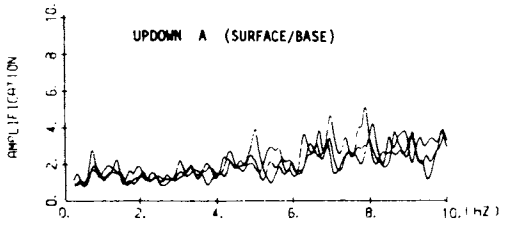

Fig. 32 FRF (Amplification) of A to A67 in Vertical (Tsuchida et al (1978))

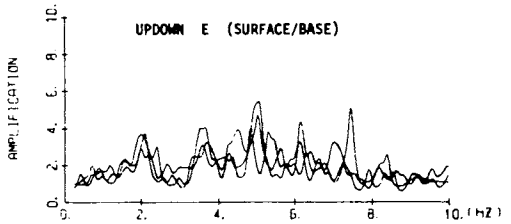

Fig. 33 FRF (Amplification) of E to E50 in Vertical (Tsuchida et al (1978))

There may be many possible seismic wave propagation models which are not contradictory to the observations. One of the possible models is the multiple reflection of shear waves in the vertical direction at each site. FRF of the points A and E based on the multiple reflection theory was calculated, and the results are shown in Fig. 36. The peak frequencies of FRF from the earthquake observation (Fig. 30 for point A, and Fig. 31 for point E) and those from the multiple reflection theory (Fig. 36)

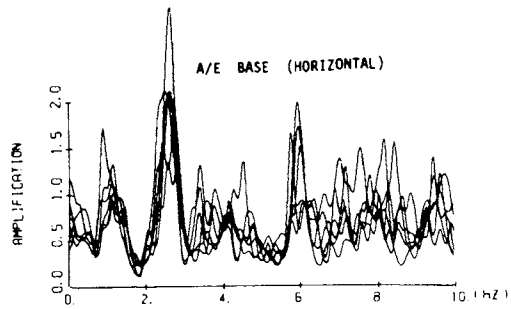

Fig. 34 FRF (Amplification) of A67 to E50 in Horizontal (Tsuchida et al (1978))

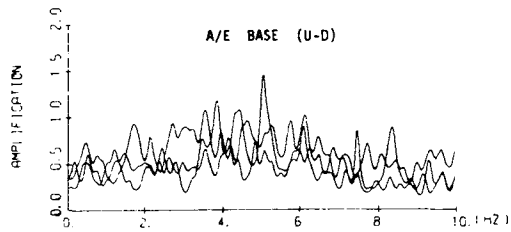

Fig. 35 FRF (Amplification) of A67 to E50 in Vertical (Tsuchida et al (1978))

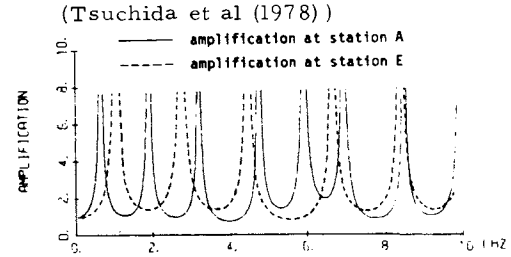

Fig. 36 FRF (Amplification) of Multiple Reflection Model with No Damping (Tsuchida et al (1978))

agree very well, especially for the three lower natural frequencies. Shear wave velocities used for the analysis were measured from the shear wave propagation in the vertical. This agreement will support the concept that seismic waves propagate vertically in a surface layer.

The earthquake ground motions at the points A67 and E50 are not identical as it is understood from Fig.34. Therefore, the incident waves were calculated with the multiple reflection theory and compared in form of FRF between the points A67 and E50. The results are shown in Fig.37. From this it is found that the calculated incident waves are not identical, either. The figure

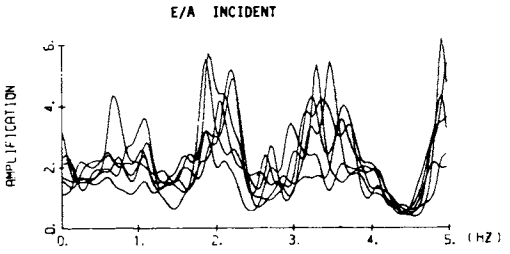

Fig. 37 FRF (Amplification) between E and A (Calculated Incident Waves) (Tsuchida et al (1978))

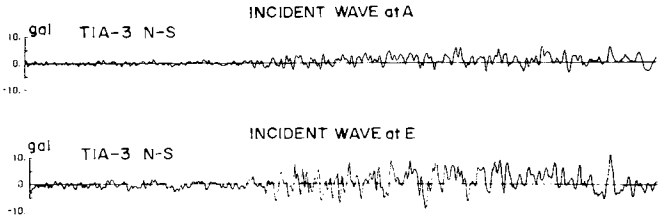

Fig. 38 Incident Accelerations at Points A and E (Tsuchida et al (1978))

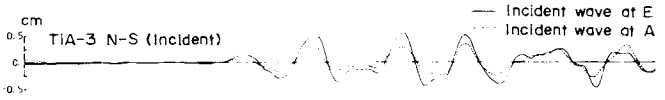

Fig. 39 Incident Displacements at Points A and E (Tsuchida et al (1978))

indicates that there are some correlations between the incident waves at the two points regardless of the earthquakes and the components in the horizontal directions. The acceleration time histories of the incident waves at the two points are compared in Fig.38.

The displacement time histories were calculated from the acceleration time histories and shown in Fig.39, which indicates that the agreement in the low frequency component is rather good. The same can be read from Fig.37, although FRF seems to be emphasizing the difference comparing with the time histories. Therefore, when only low frequency components of earthquake ground motions are of importance, the multiple reflection theory of seismic shear waves in vertical direction seems to be one of the applicable approaches.
In conclusions, Tsuchida et al (1978) points out that the multiple reflection theory is not contradictory to the results of the observation, and that the frequency response functions calculated with shear wave velocities measured at the site and based on the theory of multiple reflection agreed very well with the frequency response functions calculated from the observed earthquake records.

Local Laboratory Array at PWRI in Tsukuba

The Public Works Research Institute (Sakagami et al (1980), Okubo et al (1980)) installed in 1979 a local laboratory array in Tsukuba, Ibaraki Prefecture for observing characteristics of propagation of seismic waves and seismic ground strains in the horizontal and vertical directions. One of important objectives of this array observation is to obtain appropriate information for the seismic design of underground pipelines whose seismic stresses may be mainly induced by the propagation of the ground strain during earthquakes.

PWRI in Tsukuba is located about 60 km north of Tokyo as shown in Fig.40. The figure also shows the location of Ashitaka Area in Numazu City, Shizuoka Prefecture, where a simple extended array is operated by PWRI (see the following section).

Fig.41 illustrates the entire plan of PWRI in Tsukuba, where two local laboratory array fields are shown by Field-A and Field-B. At Field-C in the southern end a 3-component strong motion accelerometer having autodial data transmission system is installed. Fig. 42 is a bird-eye view of the northern half of PWRI, indicating Field-A, Field-B, the main office building and a building with the central processing room of strong-motion earthquake records obtained in the fields. Fig. 43 shows the configuration of locations of 20 three-component accelerometers.

In the Field-A equipped are 13 three-component accelerometers, consisting of 7 on the surface 1 at the depth of 2 m and 5 at the depth of 50 m, along a cross-shape configuration with the length of 100 m from south to north and from east to west. In the Field-B installed are 6 three-component accelerometers, 1 at the depth of 2 m, 4 at the depth of 66 m and 1 at the depth of 96 m, along a L-shape configuration with short and long length of 50 m and 100 m, respectively. Table XII is a list of the 20 accelerometers. The directions of the cross and L-shape configurations are oriented along north to south and east to west. The directions of the components of accelerometer sensors are the same.

Main specifications of the accelerometers used are summarized in Table XIII. Signals of the all sensors are transmitted by underground cables to the data processing room of strong-motion earthquake records via field station houses.

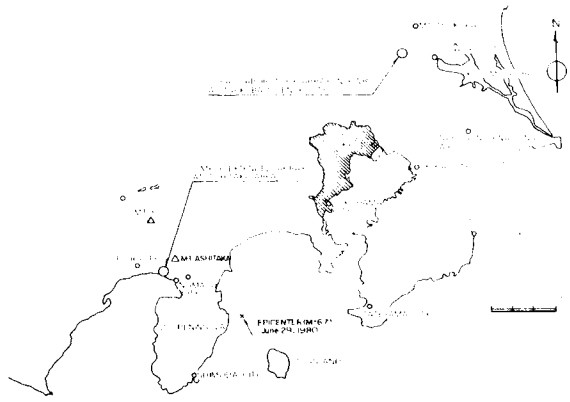

Fig. 40 Two Locations of Dense Strong-Motion Arrays Operated by PWRI

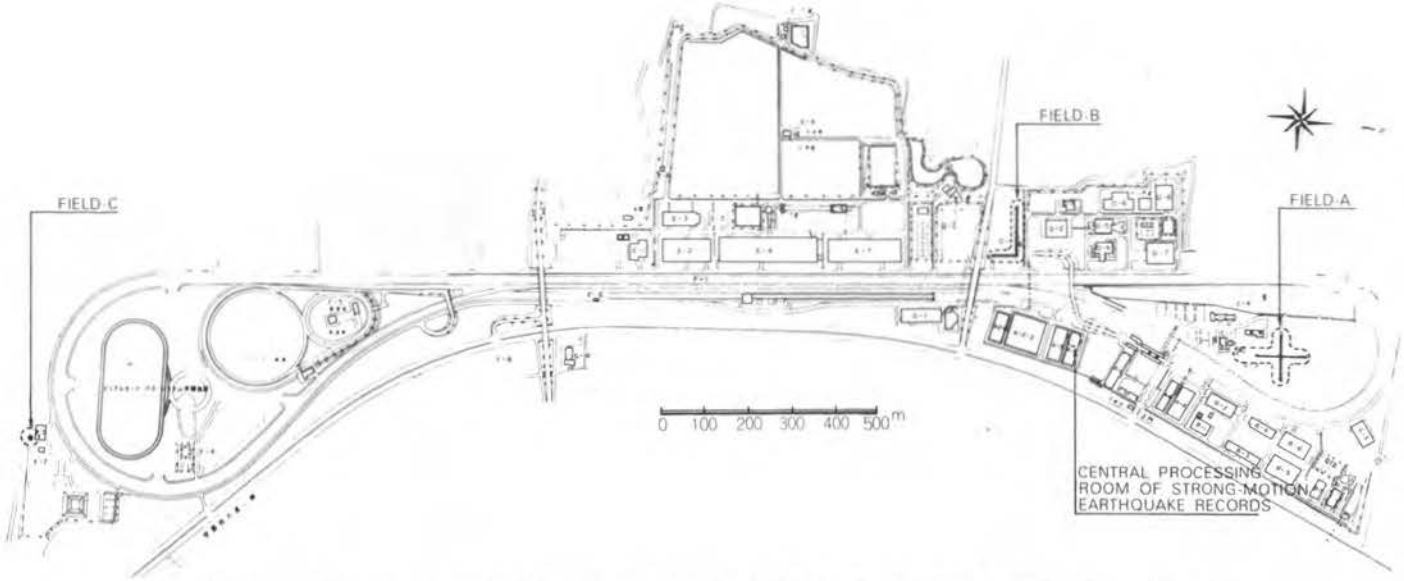

Fig. 41 Fields of Local Laboratory Array at PWR1 in Tsukuba, Ibaraki Prefecture

Fig. 42 Bird-eye View of Local Laboratory Array at PWR1

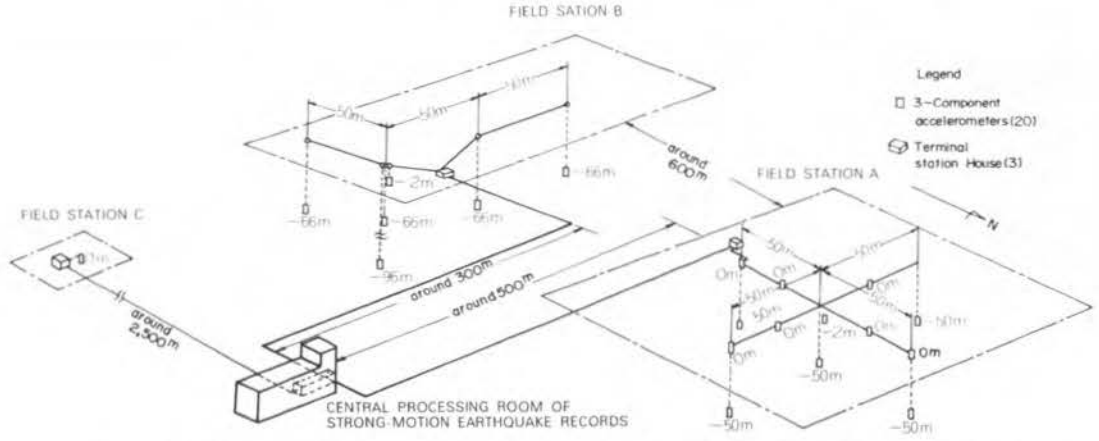

Fig. 43 Locations of Accelerometers of Local Laboratory Array at PWR1

At the Fields A and B triggering of seismic records is performed either when the peak vertical acceleration exceeds 3 gals at both Fields (one of the 50 m-depth points at Field A and 96 m-depth point at Field B) or when the peak horizontal acceleration at one of the two points exceeds 5 gals.

At Field C which has a 3-component accelerometer with specifications shown in Table XIII, triggering is done when the peak vertical acceleration exceeds 3 gals.

Geological conditions around the Institute are found to be rather uniform in the horizontal, as shown in Fig. 44. Fig. 45 shows a soil profile of the area up to the depth of 250 m. Standard penetration resistances (N-values) are provided up to the depth of 100 m. From these it is seen that loam soils cover the surface of the entire area near the Institute with a thickness of about 5 m, and that alluvial sandy and silty deposits of approximate thickness of 50 m rest on diluvial gravel formation. Shear wave velocities of the alluvial and diluvial deposits are measured to be about 250 and 400 m/sec, respectively, in this area. It is estimated that a rocky layer exists deeper than several hundred meters.

Table XII Numbers of Accelerometers and Components of Strong-Motion Array at PWRI

Field	Depth	Points	Components
Field-A	Ground Surface	7	21
	-2m	1	3
	-50m	5	15
Field-B	-2m	1	3
	-66m	4	12
	-96m	1	3
Field-C	Ground Surface	1	3
Total		20	60

Table XIII Specifications of Accelerometers in Local Laboratory Array at PWRI

Number of Component	3
Type	Velocity Feed Back
Natural Frequency	5 Hz
Frequency Range	0.1 - 50 Hz ; within 1 dB
Maximum Acceleration	± 650 gals
Diameter, Length	ϕ 13 cm, 125 cm
Weight	50 kg

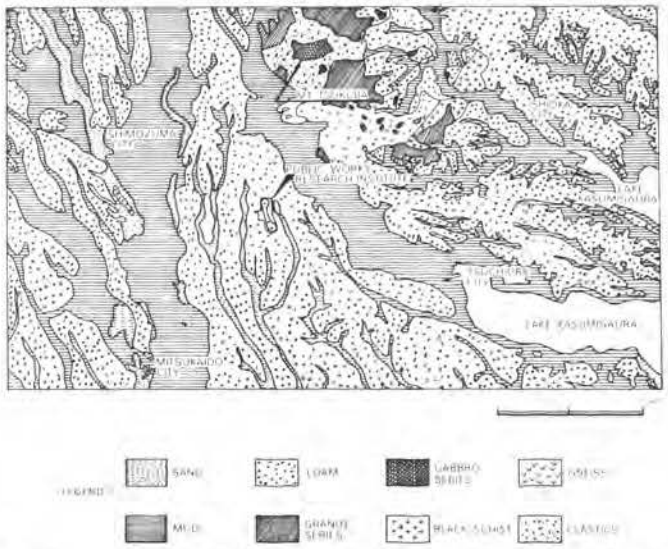

Fig. 44 Surface Geological Map Around Public Works Research Institute in Tsukuba Science City (After Reference 5)

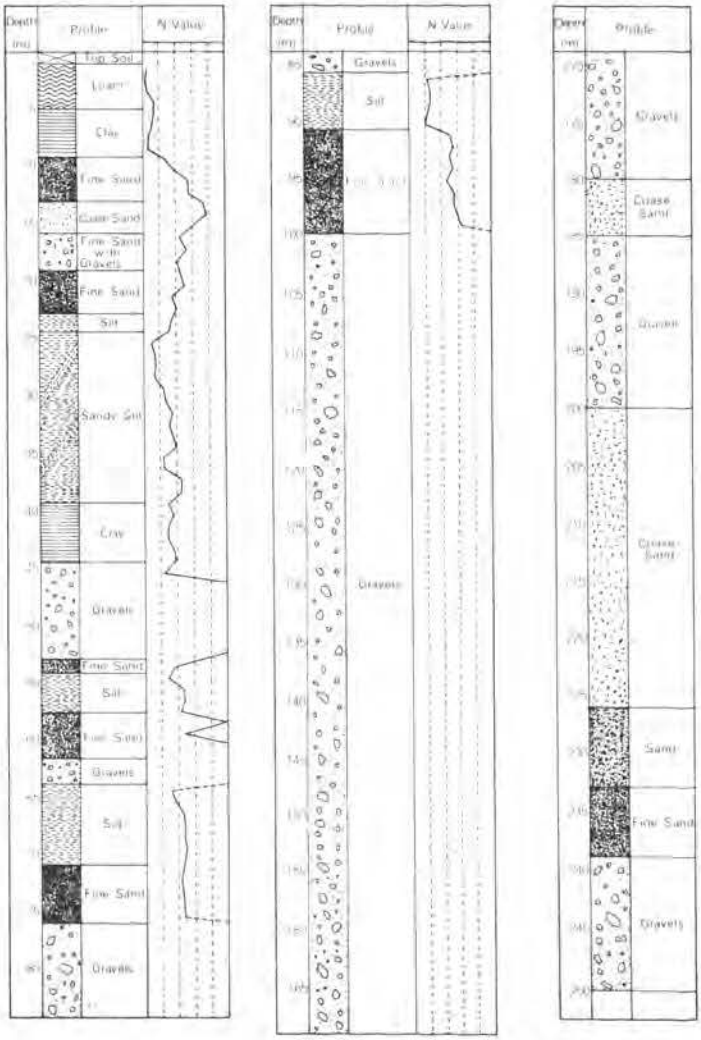

Fig. 45 Soil Profile at PWRI in Tsukuba Science City

Signals from the twenty accelerometers installed at Fields A, B, and C are recorded on a magnetic tape of a computer system equipped in the data processing room. Flow of the data processing system (see Fig. 46) is outlined as follows:

(1) Except for 21 signals of the 7 surface accelerometers at Field A, 36 signals of Fields A and B are automatically digitized with a time interval of 1/100 sec by an A-D converter and stored on a magnetic disk with the maximum capacity of 64 MB with use of a computer system having a core memory of 80 KW. Pre-event memories of 5 sec are prepared for the 36 signals so that entire recording of earthquake motions may be achieved. Data stored on the magnetic tape are compiled into a form of standard data processing of strong-motion records, and stored on a magnetic tape. Besides this recording system, an analog tape recording system is also supplimentarily provided to store 32 signals out of 36.

(2) The 21 signals of the surface accelerometers at Field A are automatically digitized with a time interval of 1/100 sec by an A-D converter and stored on a magnetic disk. Pre-event memories are not provided for the 21 signals. But the simultaneity of time code of the 21 signals with that of the 36 signals is kept.

(3) The 3 signals of an accelerometer at Field C is automatically digitized with a time interval of 1/100 sec by an A-D converter and stored on a digital cassette tape. Pre-event memories of 10 sec are provided. After an earthquake, a transmitter at Field-C automatically calls for an extension of the central data processing room as much as three times. If a connection is achieved within one of the three calls, the data recorded on a digital cassette tape are transmitted to a magnetic disk of the computer system in the processing room via telephone call. If a connection cannot be achieved within three times, the transmitter gets into a stage of waiting and keeping the data.

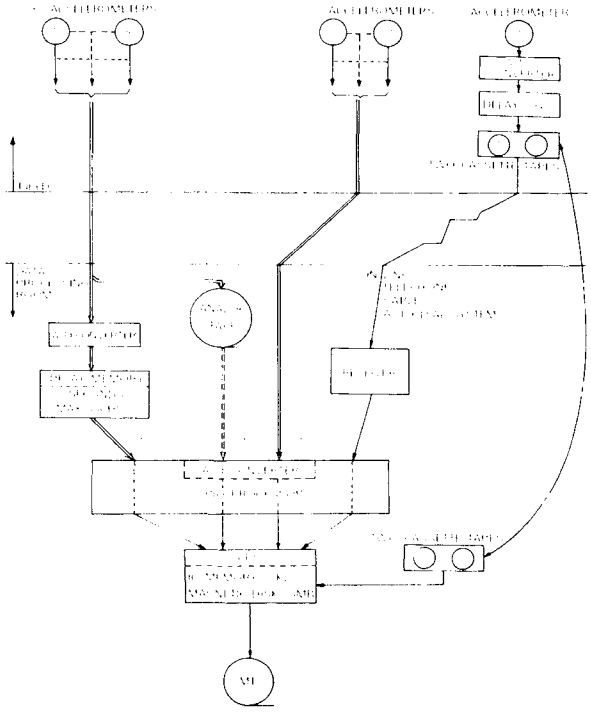

Fig. 46 Data Processing System

For analyzing thus recorded motions, a computer system with a core memory of 192 KW is provided as shown in Fig. 47. Transmission of the data from the recording system to analyzing system is performed on a tape basis. This computer system is designed for the use for the analysis of the data obtained through the PWRI strong-motion observation network throughout Japan, as well as the data obtained from the Fields A, B and C in Tsukuba.

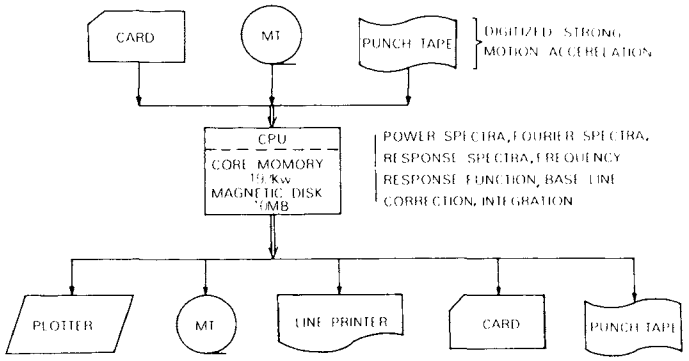

Fig. 47 Data Analyzing System

During an earthquake of July 11, 1979 with the Richter magnitude of 5.9, focal depth of 40 km, and an epicentral distance of 120 km, the recording system took the first records. Fig. 48 represents acceleration records at the north, east, south, and west edges of the cross with the depth of 50 m in the Field-A. These records are designated as N50, E50, S50, and W50 as shown in Fig. 49.

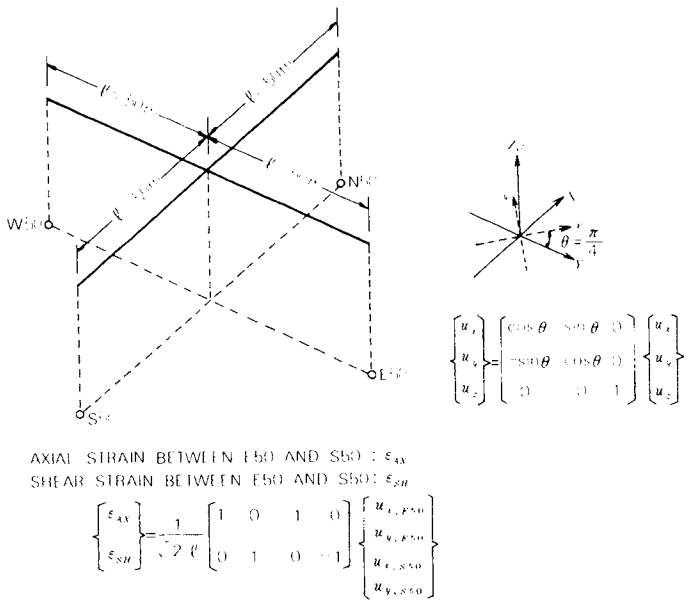

Fig. 49 Definition of Axial and Shear Strains between Two Points

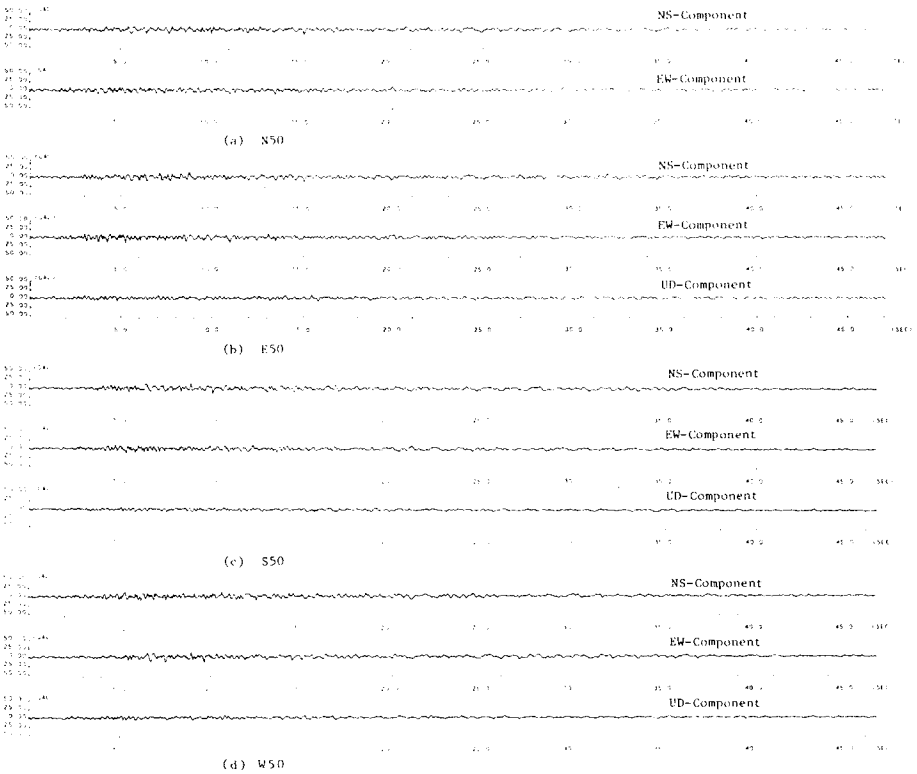

Fig. 48 Acceleration Records at N50, E50, S50 and W50 at Field-A of Local Laboratory Array of PWR1 in Tsukuba

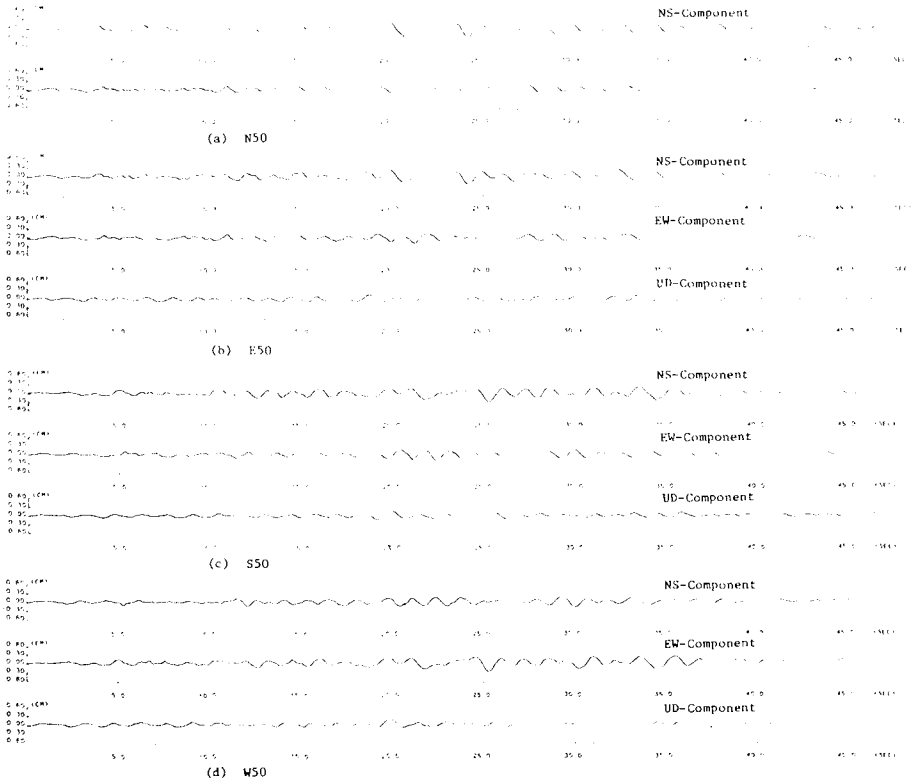

Fig. 51 Displacements Calculated from Acceleration Records at N50, E50, S50, and W50 at Field-A of Local Laboratory Array of PWR1 in Tsukuba

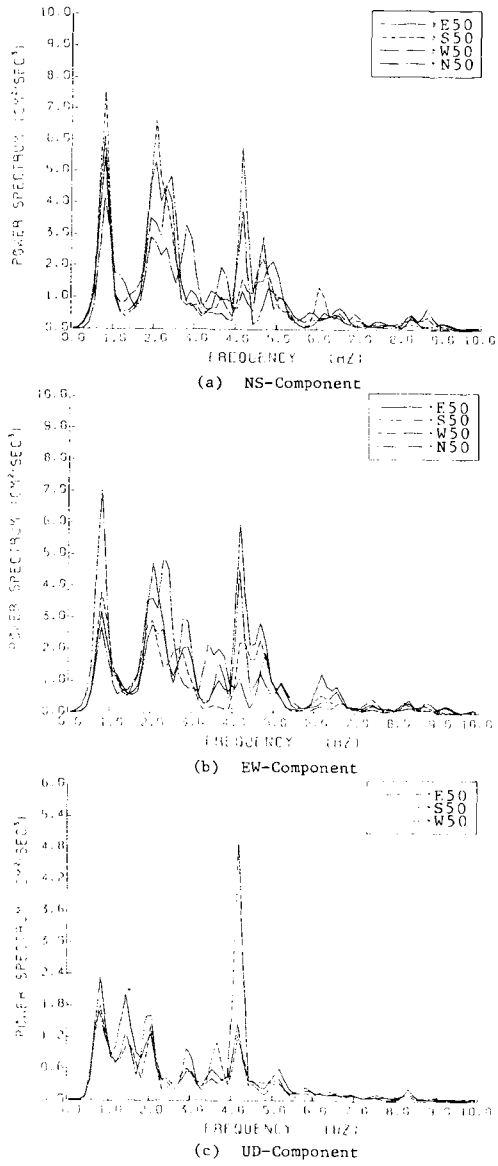

(a) NS-Component

(b) EW-Component

(c) UD-Component

Fig. 50 Power Spectra of Acceleration Records Obtained At N50, E50, S50, and W50

Fig. 50 illustrates power spectra of the acceleration records, and Fig. 51 represents displacement time histories computed by double integration of the acceleration time histories.

Ground strains induced by the earthquake were estimated by using the displacements shown in Fig. 51. An average ground strain between two observing points are defined as

$$\begin{Bmatrix} \varepsilon_{Ax} \\ \varepsilon_{SH} \end{Bmatrix} = \frac{1}{L} \begin{bmatrix} 1 & 0 & -1 & 0 \\ 0 & 1 & 0 & -1 \end{bmatrix} \begin{Bmatrix} u_{1,i} \\ u_{2,i} \\ u_{1,j} \\ u_{2,j} \end{Bmatrix} \tag{11}$$

where ε_{Ax} and ε_{SH} denote average axial strain and shearing strain between the specified two points, respectively, and U_1, k and U_2, k (k=i, j) represent ground displacements at point k in the NE-SW and NW-SE directions, respectively. A parameter L is defined as a length between the two point and is given by $\sqrt{2}\,\ell$ in this case, where ℓ =50m.

Displacements U_1, k and U_2, k (k=i, j) can be determined in the form

$$\begin{Bmatrix} u_{1,i} \\ u_{1,j} \\ u_{2,i} \\ u_{2,j} \end{Bmatrix} = \frac{1}{\sqrt{2}} \begin{bmatrix} 1 & 1 & 0 & 0 \\ -1 & 1 & 0 & 0 \\ 0 & 0 & 1 & 1 \\ 0 & 0 & -1 & 1 \end{bmatrix} \begin{Bmatrix} u_{NS,i} \\ u_{EW,i} \\ u_{NS,j} \\ u_{EW,j} \end{Bmatrix} \tag{12}$$

where $u_{NS,k}$ and $u_{EW,k}$ (k=i, j) denote displacements at point k in the N-S and E-W directions, respectively.

According to eqs. (11) and (12), average axial strain ε_{Ax} and shearing strain ε_{SH} were computed between N50 and W50, and between E50 and S50. The results are shown in Fig. 52. The peak value of both ε_{Ax} and ε_{SH} are estimated as approximately 5×10^{-5}. One can approximately estimate the average strain from displacements shown in Fig. 51, assuming that the displacements on joints i and j are in out-of-phase. Because the peak displacements in Fig. 51 are approximately 0.3 cm, the average strain based on the above assumption can be estimated as

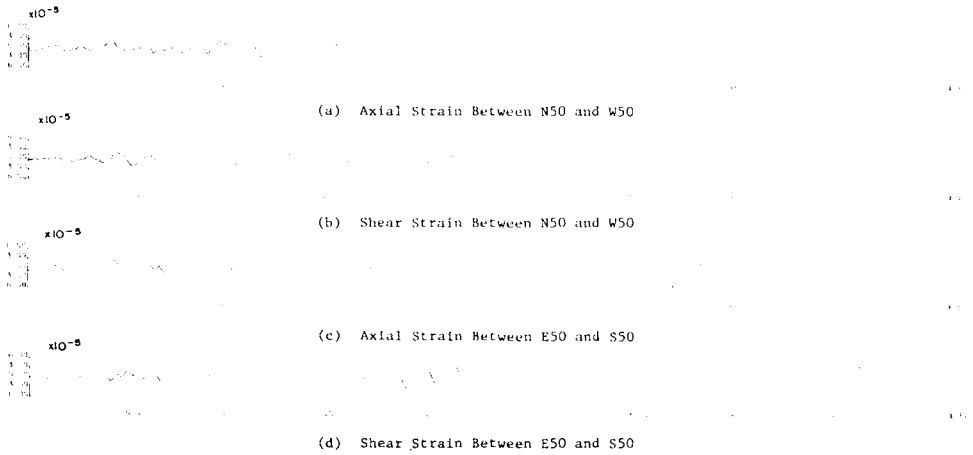

(a) Axial Strain Between N50 and W50

(b) Shear Strain Between N50 and W50

(c) Axial Strain Between E50 and S50

(d) Shear Strain Between E50 and S50

Fig. 52 Axial and Shear Strains Between Two Points

$$\varepsilon = \frac{2u_{max}}{L} = \frac{2 \times 0.3}{\sqrt{2} \times 5000} \fallingdotseq 8.5 \times 10^{-5} \qquad (13)$$

which is close to the strains determined by eq. (11).

Simple Extended Array at Ashitaka Area

PWRI (Sakagami et al (1980), Okubo et al (1980)) has recently deployed a simple extended array at Ashitaka area, which is located between Numazu City and Fuji City in Shizuoka Prefecture, as shown in Fig. 40. This array observation is to quantitatively evaluate the effects of geological conditions on ground motions. Fig. 53 shows the surface geological map around that area. The surfaces of this area are covered by gravels near the ocean, by loam in the mountain foot, and by peat in the middle. Geological features change very intensely at the array location as seen in Fig. 53.

Fig. 54 and 55 indicate the cross section and the plan at the array location, respectively. In Fig. 54 geological section estimated by nine boring logs along this line is also shown. As seen in the figures important traffic facilities such as National Highway Route 1, Bypass of Route 1, Tokaido Line (Railway), and Shinkansen (New Trunk Line) run in the area in the east-west direction. The array consists of five strong-motion accelerographs, one on a sand dune facing Suruga Bay, three on peat, and one on loam of the foot of Mountain Ashitaka. Four points (1, 2, 3, and 5) were completed in March, 1980, and one point (4) in October, 1980. Principal specifications of the accelerographs are summarized in Table XIV.

Accelerations up to ± 1g can be recorded, and signals are digitized with a time interval of 1/200 sec, storing on a digital cassette tape. Time code generators are equipped in all the five recording systems so that exact triggering time can be recorded at the five sites.

Table XIV Specifications of Accelerograph Used for Simple Extended Array at Ashitaka Area (DSA-1 Type)

Accelerometer	Type	Triaxial, Force Balance
	Full Scale Range	± 1G
	Natural Frequency	50 Hz
	Damping	70% critical
Trigger System	Sensitive Direction	Vertical
	Acceleration Set Point	0.01G
	Operation Cycle	Self-actuating for duration of earthquake, with automatic reset
Recording System	Type	Digital, phase encoded
	Number of Track	4
	Mangetic Tape	Digital cassette tape; 2.5inch/sec.
	Frequency Response	DC ~ 30 Hz; -12 dB/oct
	Number of Bits	12 bits
	Dynamic Range	> 66 dB
	Sampling Rate	200 Samples/sec/channel
Power Requirements	Voltage	± 12 VDC
	Battery Charger	Float charger supplied
Time Code Generator	Accuracy of Crystal Controlled Time	$> 1 \times 10^{-6}$
	Auto Adjustment of Time of Crystal	Each 5 seconds by JST Standard Time

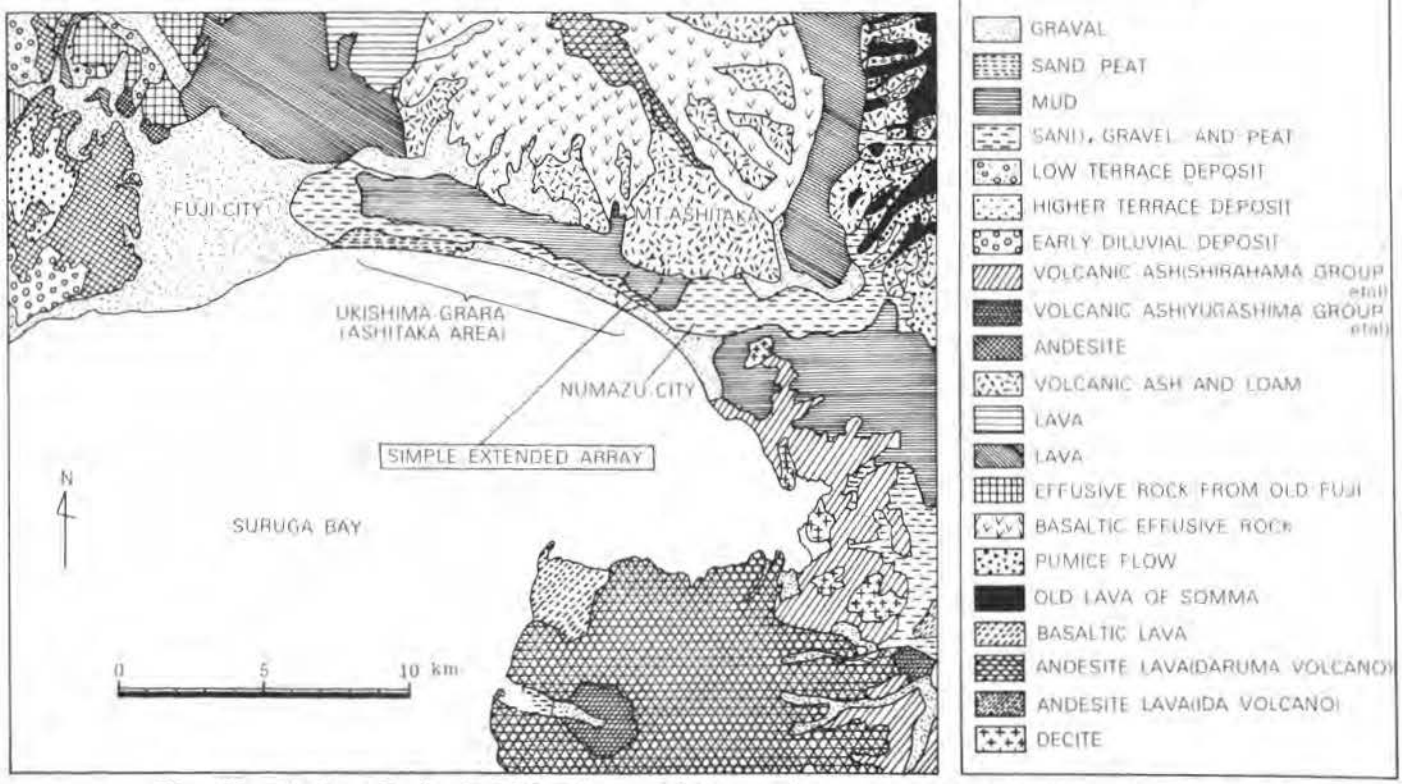

Fig. 53 Surface Geological Map Around Ashitaka Area. Numazu City, Shizuoka Prefecture

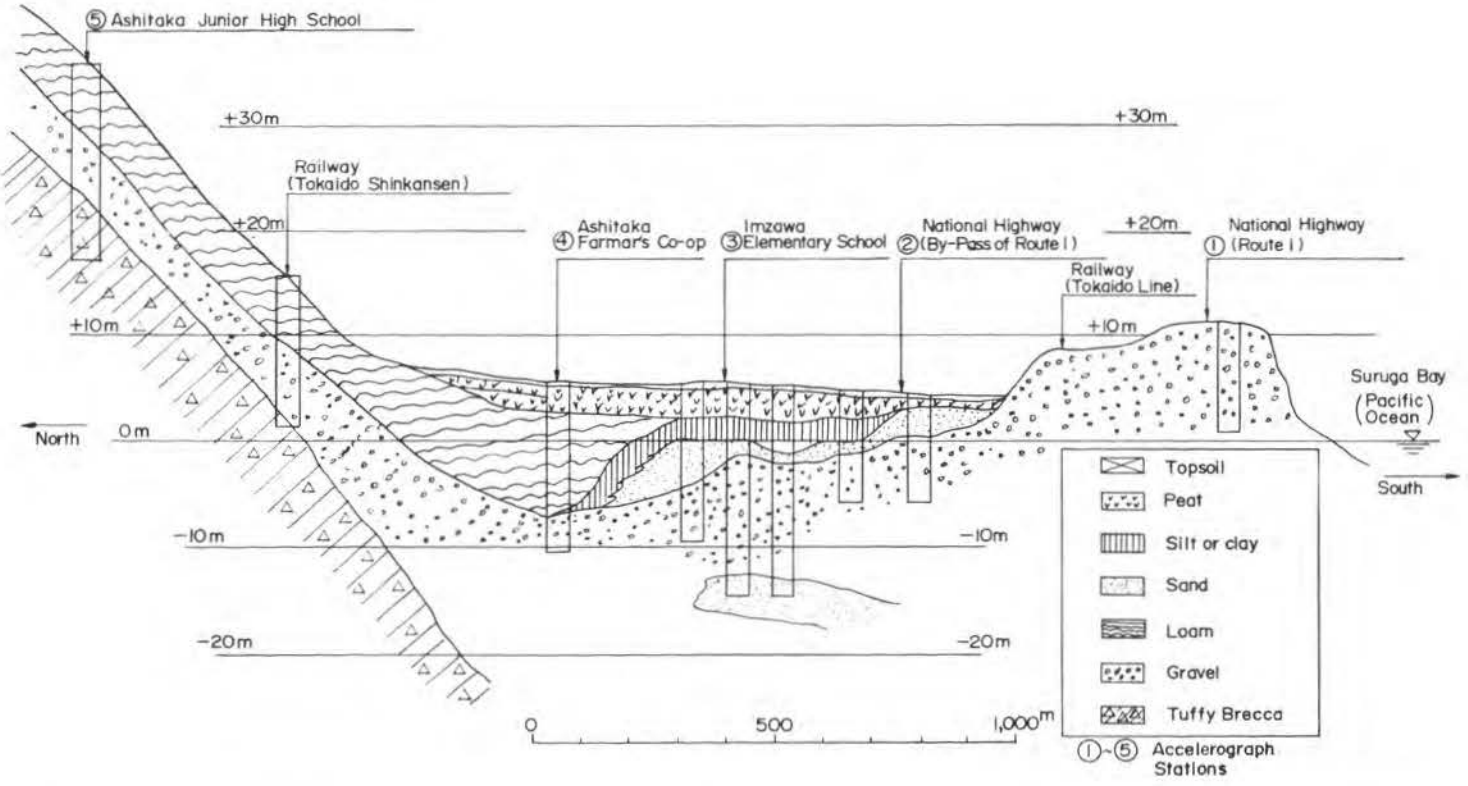

Fig. 54 Accelerograph Stations at Simple Extended Array at Ashitaka Area, Numazu, Shizuoka Prefecture

Fig. 55 Aerial View of Simple Extended Array at Ashitaka Area, Numazu, Shizuoka Prefecture

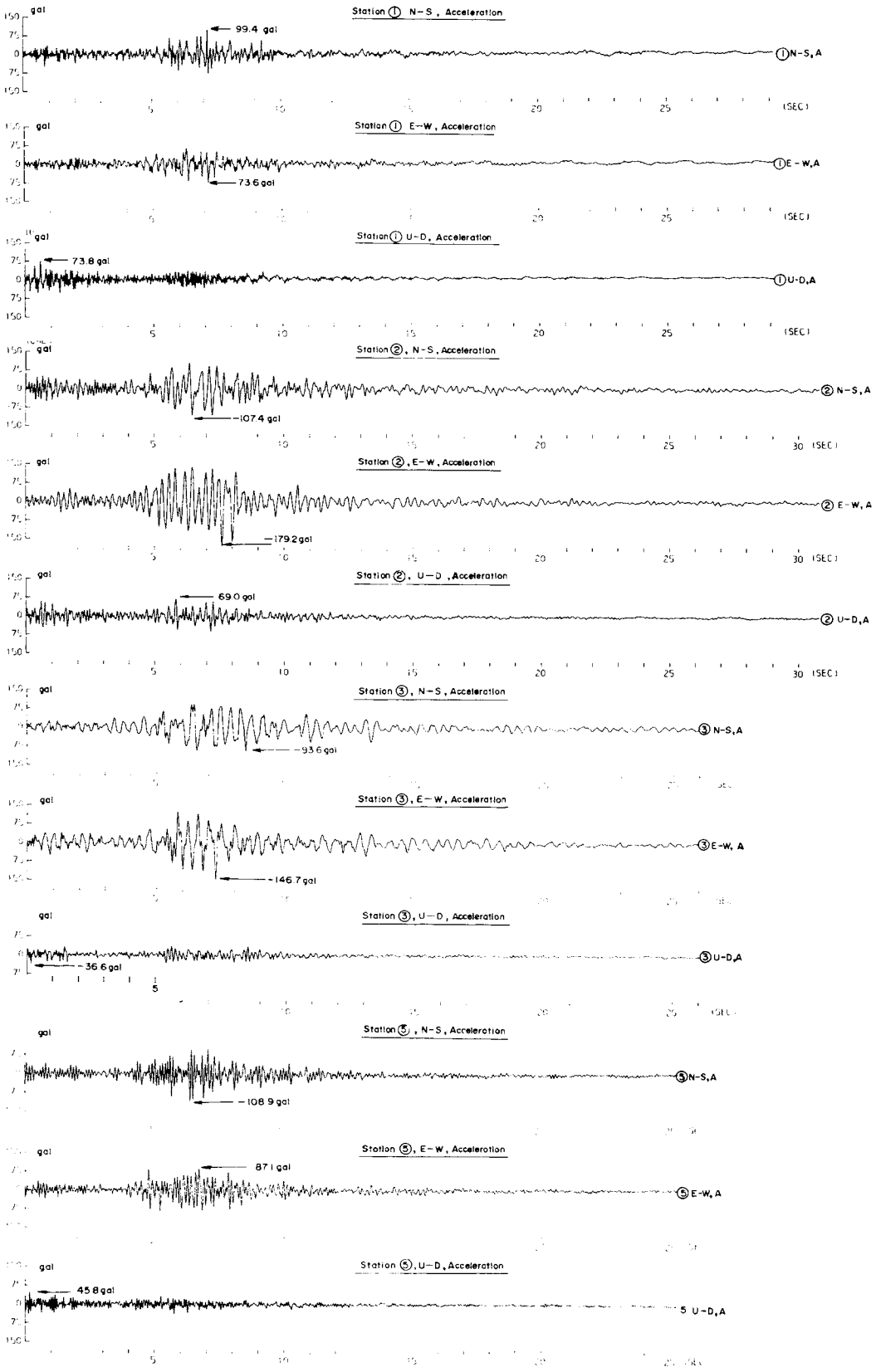

Fig. 56 Acceleration Records At Four Stations During the Izu Peninsula Earthquake of June 29, 1980 (M=6.7, $\Delta \doteqdot 45$ km)

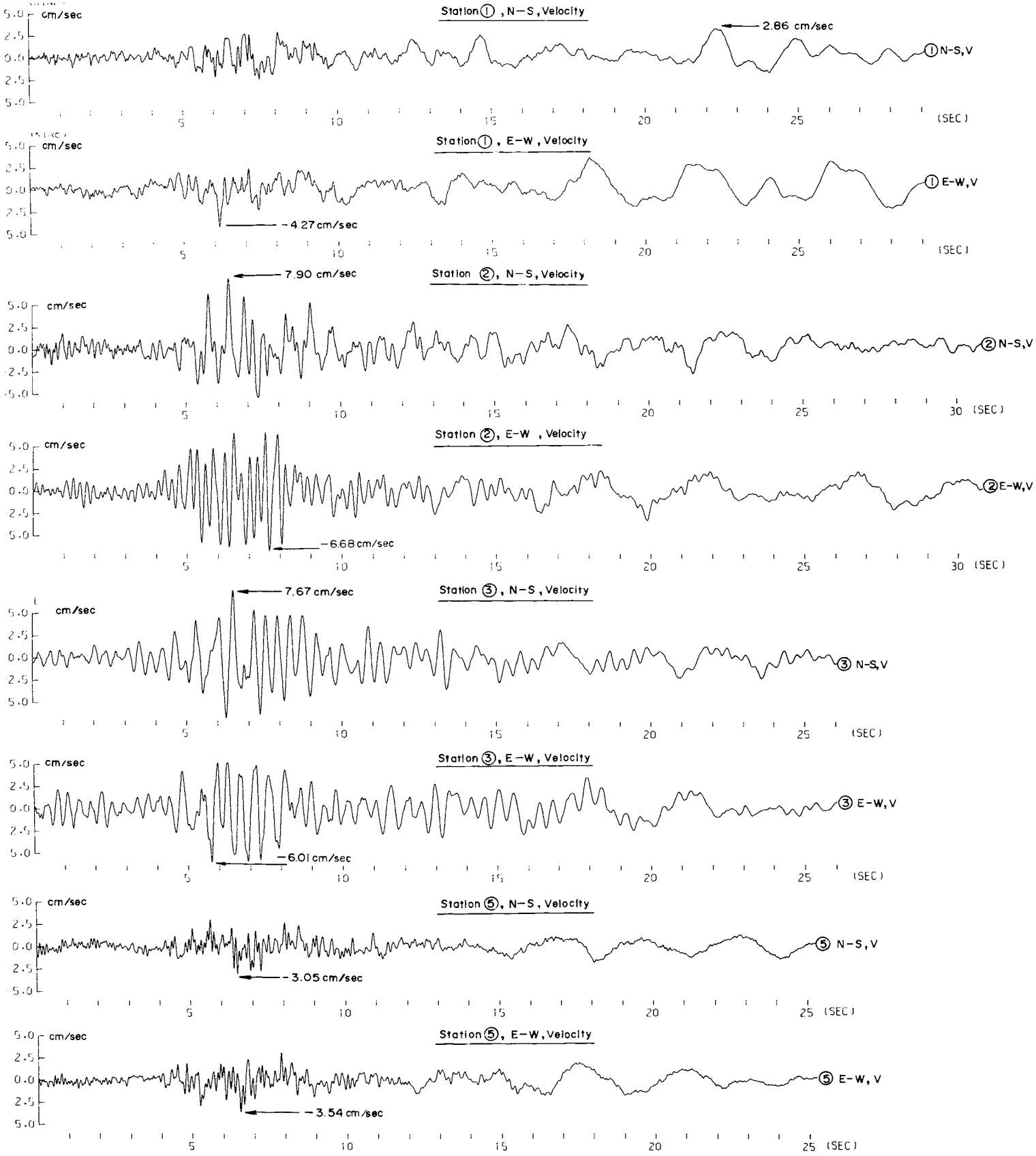

Fig. 57 Velocities Calculated from Acceleration Records at Four Stations During the Izu Peninsula Earthquake of June 29, 1980 (M=6.7, $\Delta \div 45$ km)

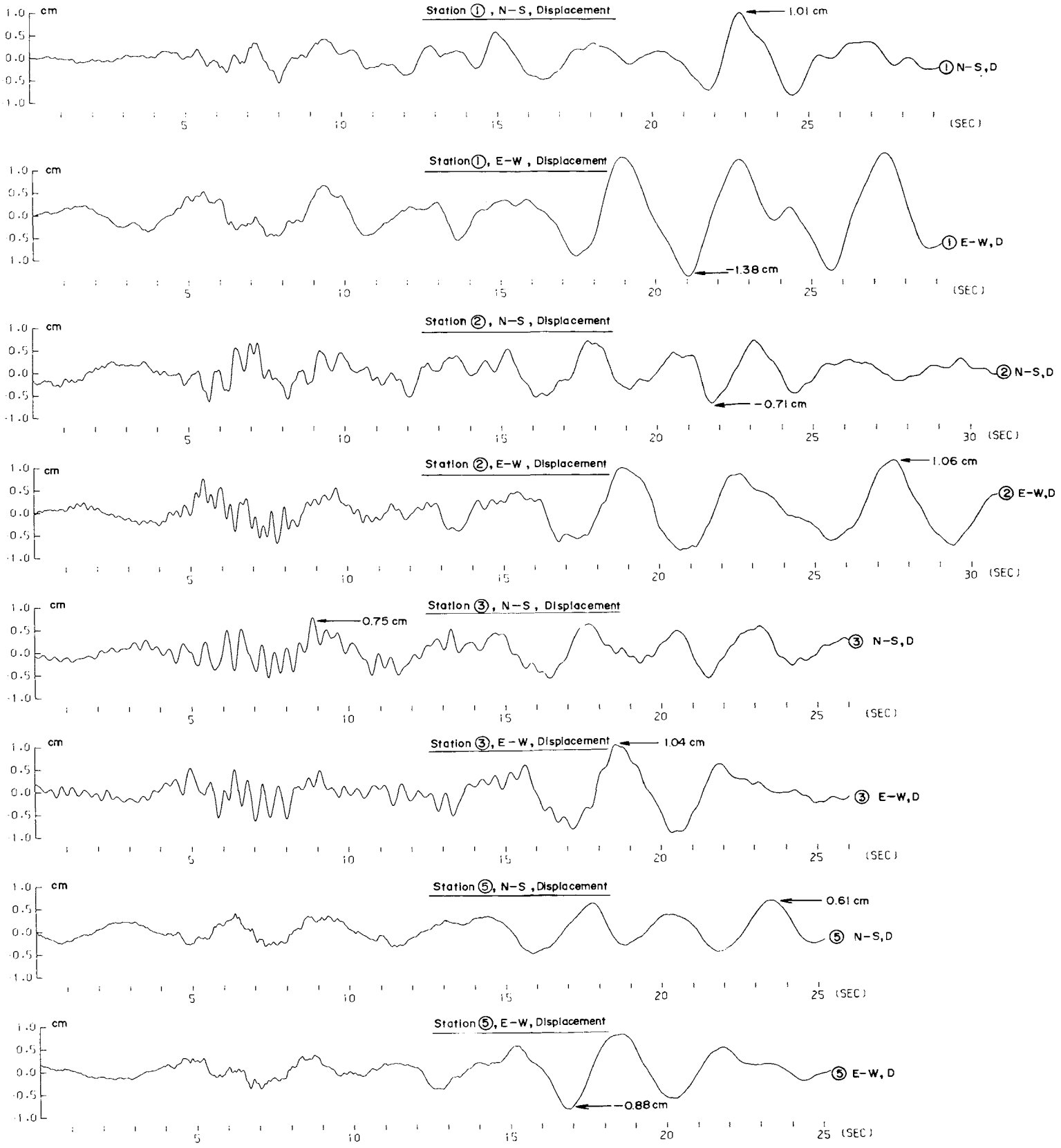

Fig. 58 Displacements Calculated From Acceleration Records at Four Stations During the Izu Peninsula Earthquake of June 29, 1980 (M=6.7, $\Delta \div 45$ km)

On June 29, 1980 a magnitude 6.7 earthquake broke off under the sea bottom off Izu Peninsula. The epicenter is shown in Fig. 40. The hypocentral depth was very shallow. The epicentral distance to the array stations was about 45 km. Four accelerographs at stations 1, 2, 3 and 5 triggered complete accelerations. Fig. 56 illustrates 12-component accelerograms at the four stations. Figs. 57 and 58 indicate calculated velocities and displacements of the eight horizontal components, respect-

Table XV Peak Accelerations, Velocities, and Displacements and Times of Their Occurrences

Station	Component	Acceleration (gal)	Velocity (cm/sec)	Displacement (cm)
1	N-S	99.4 (7.2 sec)	2.86 (22.3 sec)	1.01 (22.8 sec)
	E-W	-73.6 (7.2)	-4.27 (6.2)	-1.38 (21.0)
	U-D	73.8 (0.6)	2.14 (10.0)	-0.70 (9.7)
2	N-S	-107.4 (6.5)	7.90 (6.4)	-0.71 (21.8)
	E-W	-179.2 (7.6)	-6.68 (7.7)	1.06 (27.5)
	U-D	69.0 (5.8)	2.67 (5.9)	-0.57 (9.1)
3	N-S	-93.6 (8.4)	7.67 (6.5)	0.75 (8.9)
	E-W	-146.7 (7.3)	-6.01 (5.8)	1.04 (18.6)
	U-D	-36.6 (0.1)	-1.86 (8.3)	-0.60 (9.0)
5	N-S	-108.9 (6.4)	-3.05 (6.6)	0.61 (23.5)
	E-W	87.1 (6.7)	-3.54 (6.5)	-0.88 (16.9)
	U-D	45.8 (0.2)	1.55 (5.6)	0.48 (6.9)

Note) Values in the parentheses indicate times of occurrence of peak values in sec, relative to the starting time of recording.

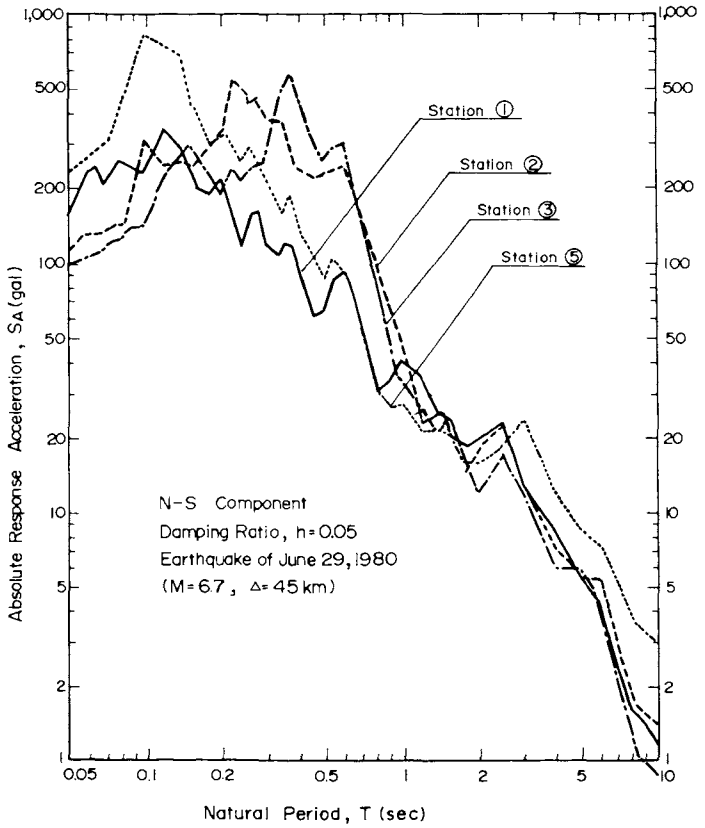

Fig. 59 Absolute Response Acceleration Spectra, N-S Components

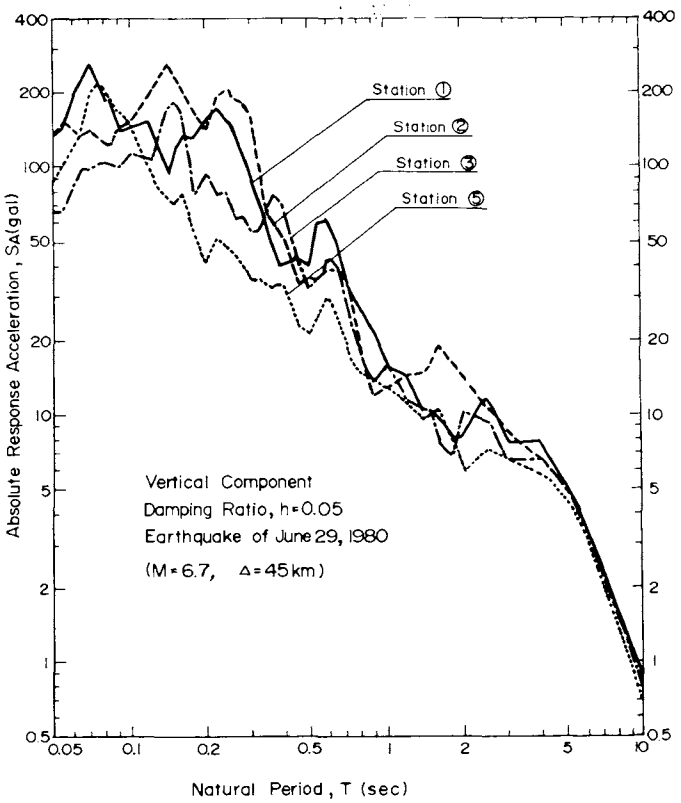

Fig. 60 Absolute Response Acceleration Spectra Vertical Components

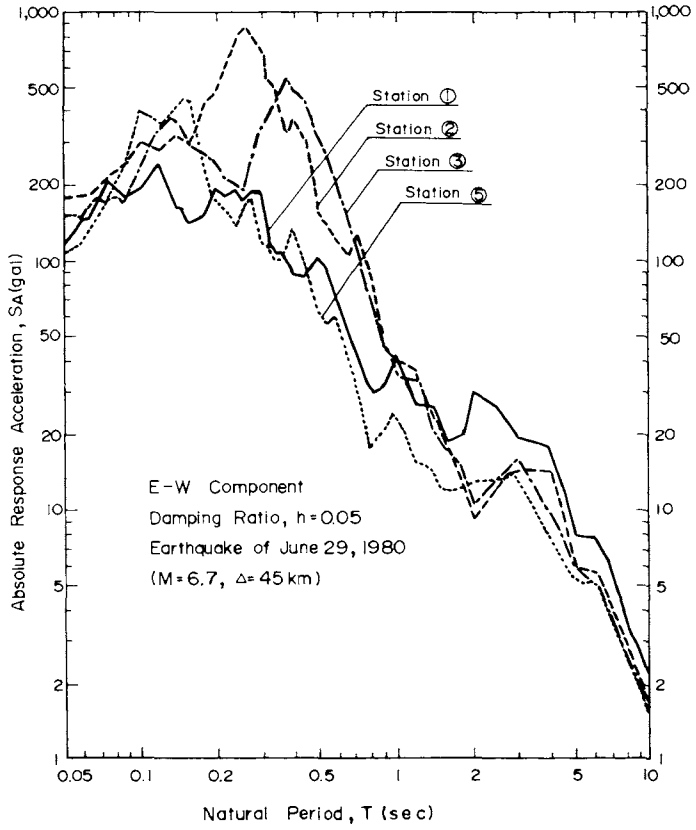

Fig. 61 Absolute Response Acceleration Spectra, E-W Components

ively. Table XV tabulates the peak values of the 12-component accelerations, velocities, and displacements, and times of their occurrences.

Figs. 59 to 61 show absolute response acceleration spectral curves for a SDOF system with a damping ratios of 5 % of critical, for N-S components, vertical components, and E-W components, respectively. Furthermore, Fig. 62 to 64 show frequency response function (Amplification of power spectrum density of station 1 to that of the other stations) in the three directions, to illustrate frequency components of the three stations with respect to those of station 1. Station 1 was taken as the basis, because the station seems to be least amplified near the surface in view of soil profiles and response spectral curves. It should be noted that although some slope failures occurred near the epicenter during the Earthquake, the Ashitaka area did not sustain any damage. From these analyses, the following can be pointed out:

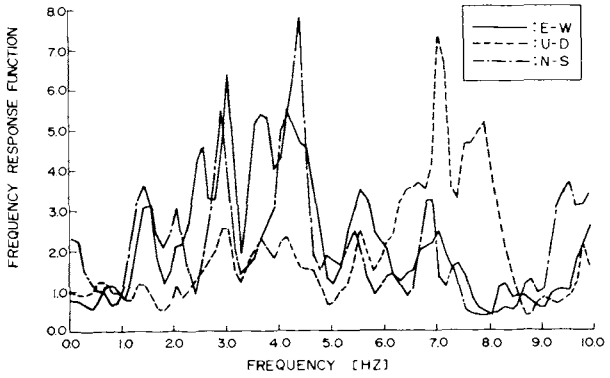

Fig. 62 Frequency Response Function of Station 2 to Station 1, for 3 Components

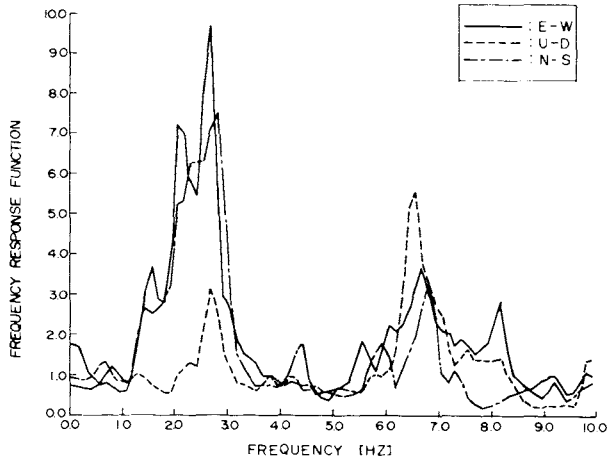

Fig. 63 Frequency Response Function of Station 3 to Station 1, for 3 Components

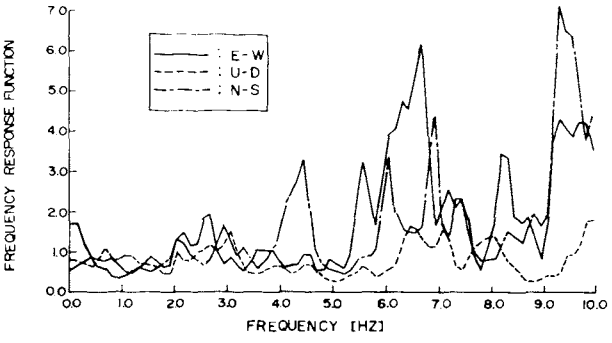

Fig. 64 Frequency Response Function of Station 5 to Station 1, for 3 Components

(1) Peak accelerations in the N-S direction are almost the same among the four stations. Peak accelerations in E-W components, however, are rather different. Accelerations at stations (2, 3) with soft soil conditions are larger than the other two (1, 5) by a factor of around 2.0. This tendency is much clearer for peak velocities. Namely, horizontal velocities at soft soils (2, 3) are greater than the other two (1, 5), by a factor of 2 to 3. Vertical velocities, however, are rather close among the four stations. Times of occurrences of peak accelerations are rather early and almost identical to those of peak velocities for the horizontal components.

(2) Peak displacements are similar among the four stations, for each of the three directions. Times of occurrences of peak displacements are rather late.

(3) By comparing horizontal response spectra (see Fig. 59 or 61) at the four stations (whose soil conditions are different) for an earthquake, it is seen that general characteristics are close. Looking at them carefully, however, one notes that responses in the range of medium period (0.2 to 0.9 sec) are predominant at the soft soil sites (2, 3), by a factor of 3 to 5. Also general shapes are very close between the two horizontal perpendicular directions (compare Figs. 59 and 61). Natural periods having peak amplitudes are 0.1 to 0.15 sec at stiff stations (1 and 5), and 0.2 to 0.4 sec at soft stations (2 and 3).

(4) Vertical response spectral amplitudes (see Fig. 60) at the four stations are generally lower than horizontal ones. Natural periods with peak response amplitudes are much shorter than the cases for the horizontal.

(5) By looking at three frequency response functions (station 1 is taken as the basis), the ordinates are generally greater than unity for the two soft stations (2, 3), but generally close to unity for the stiff station (5). At each station shapes of frequency response functions are very similar among the three components. This implies that frequency response functions do not significantly change depending on directions at one station.

(6) Frequency response functions for the stations 2 and 3 are rather high for the frequency range of 1 to 7 Hz. Those for the station 5 are almost equal to one in the same frequency range, but become higher in the high frequency range of 6 to 10 Hz.

Dense Instrument Array Programs in U.S.

In U.S., several regions have already equipped with dense instrument arrays. The Imperial Valley,

California, and Gilroy, California are better examples. The Gilroy Array recorded the Coyote Lake Earthquake of August 6, 1979 with a magnitude of M_L=5.7, and provides more than 20 strong-motion records, among which the nearest one was taken at only 2 km from the causative fault (Porcella (1980)).

The Imperial Valley array also recorded the 2nd El Centro Earthquake of October 15, 1979, and collected more than 20 records, including a record with peak vertical acceleration of 1.5 g which was taken very close to the causative fault (Brady et al (1980)).

Those records will provide designers useful informations in understanding characteristics of ground motions near earthquake sources.

SOIL-STRUCTURE INTERACTIONS OF DEEP FOUNDATIONS

Soil-structure interaction problems associated with structures with shallow foundations have been investigated by numerous investigators (Velestos (1978), for example). And the effects of soil-structure interactions are already considered in the design of building structures with shallow foundations (ATC (1978)). Therefore, in this section soil-structure interactions with deep foundations buried into soft soils will be discussed with use of recorded strong-motions (Iwasaki et al (1978), Kawashima (1980).

Fig. 65 shows a general view of Itajima Bridge investigated. The bridge has two accelerograph : one on a pier cap and the other on the ground surface nearby, about 4 400 m apart from the pier site. Fig. 66 is the soil profile at the two equipment sites. Strong-motion acceleration records during four strong earthquakes are available as shown in Table XVI. Fig. 67 is an example of the records during the magnitude 7.5 Earthquake of April, 1, 1968. It should be noted that the bridge did not sustain any damages during the four strong earthquakes.

With use of the ground-motion records, response accelerations at the pier cap was analyzed. Firstly bed rock motions were computed from the measured ground surface motions by the deconvolution procedure taking account of the strain dependence of shear moduli and damping of the subsoils. The subsoils and foundations were idealized as shown in Fig. 68, as an one-dimensional shear column model with equivalent linear soil properties and one-dimensional elastic beam supported elastically by the surrounding soils, respectively. The response accelerations of the pier were then computed by applying the bedrock motions at the bottom of the shear column model of subsoils. The comparative plots of both the measured and computed accelerations at the pier cap are shown in Fig. 69 for the Earthquake of April 1, 1968. The figure shows the very close agreements between the measured and computed responses.

From the analyses the following conclusions may be derived:

(1) Seismic responses of a deeply embedded foundation are significantly influenced by the effects of surrounding soils. Predominant frequencies which are seen in the

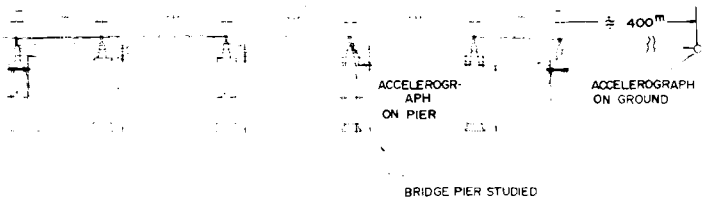

Fig. 65 General View of Itajima Bridge

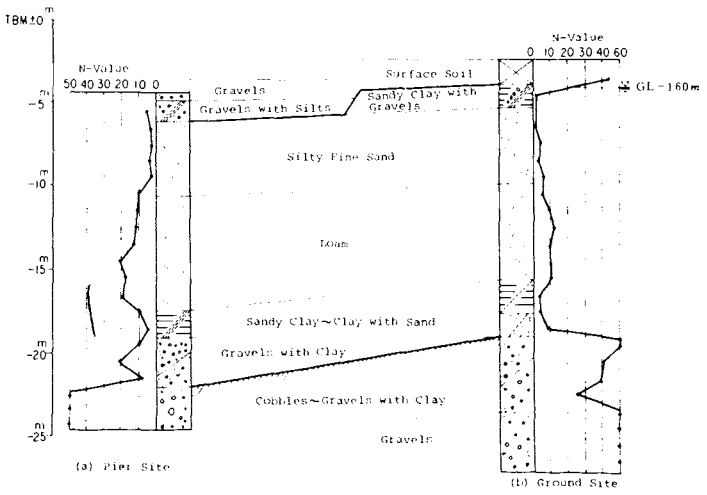

Fig. 66 Soil Profile at the Site of Itajima Bridge

Table XVI Acceleration Records at Itajima Bridge

Earthquake No.	Earthquake	Date	Richter Magnitude	Epicentral Distance (km)	Maximum Accelerations (Gal) Pier Motion		Ground Surface Motion	
					Longitudinal	Transverse	Longitudinal	Transverse
A	The Hyuganada Earthquake	April 1, 1968	7.5	100	210	310	170	186
B	The Hyuganada Earthquake (Aftershock)	April 1, 1968	6.5	100	39	66	35	42
C	The Bungosuido Earthquake	August 6, 1968	6.6	11	198	230	435	365
D	The Bungosuido Earthquake (Aftershock)	August 6, 1968	5.3	11	100	63	220	165

(Note) Longitudinal and transverse direction to the bridge axis.

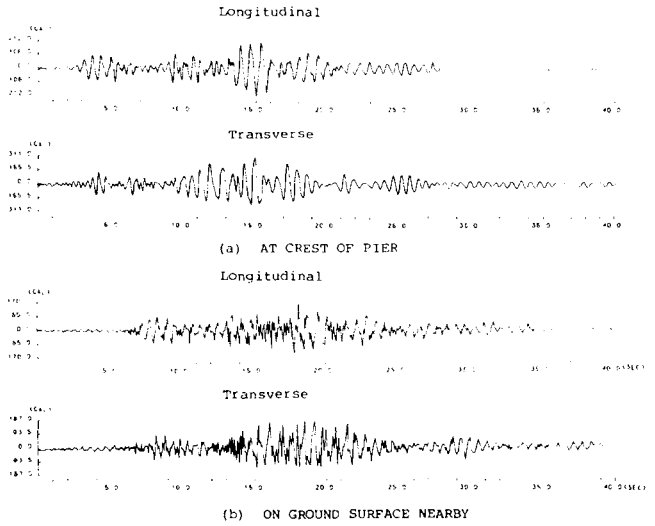

Fig. 67 Acceleration Records at Itajima Bridge During the Earthquake of April 1, 1968 (M=7.5)

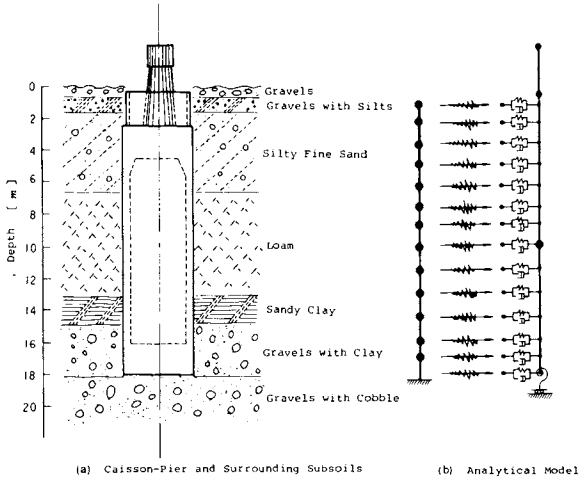

Fig. 68 Analytical Model of Foundation of the Itajima Bridge

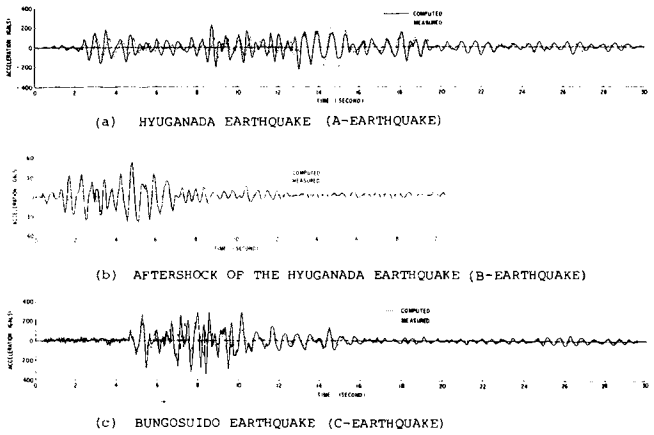

Fig. 69 Comparison of Measured and Computed Response Acceleration at Pier Cap of the Itajima Bridge

pier motions are prescribed by the lowest natural frequency of the subsurface ground so that the pier foundation responses in accordance with the motion of the subground.

(2) Seismic response accelerations of the foundation can be calculated with a good accuracy by the analytical procedure with use of the free-field ground motions measured near the foundation.

CONCLUDING REMARKS

This state-of-the-art report has described recent research findings in earthquake ground motions, rather than practical aspects of seismic structural design. Results of analyses on free field motions and structural responses are introduced with emphasis on investigations performed primarily in Japan. It seems, however, that the present status of the related studies is far from getting a consensus among the investigators.

From the viewpoint of earthquake engineering the following subjects are essential to solve the problems in ground motions and design motions: 1) Effects of Source Mechanisms and Transmission Paths, 2) Effects of Local Geotechnical Conditions, 3) Probabilistic Approach in Determining Design Seismic Loads, etc.

ACKNOWLEDGMENTS

The author wishes to experss his sincere thanks to Professor S. Prakash at the University of Missouri-Rolla, who has provided the author with an opportunity to be one of the state-of-the-art speakers of this particular International Conference.

The author wants to thank Dr. T. Okubo, Mr. E. Kuribayashi, and Mr. K. Kawashima at the Public Works Research Institute, Ministry of Construction for their supports in performing the author's investigations. He is also very grateful to Professors M. Hakuno and T. Katayama at the University of Tokyo, and Professors H. Goto, K. Toki, and H. Kameda at Kyoto University for their invaluable suggestions and discussions in completing this report.

REFERENCES

ATC (Applied Technology Council) (1978), "Tentative Provisions for the Development of Seismic Regulations for Buildings," National Science Foundation, and National Bureau of Standards.

Brady, A. G., V Perez and P. N. Mork (1980)", The Imperial Valley Earthquake, October 15, 1979, Digitization and Processing of Accelerograph Records, USGS, April.

Crouse, C. B. and B. E. Turner (1980), "Processing and Analysis of Japanese Accelerograms and Comparison with U.S. Strong Motion Data," Proceedings of the 7th World Conference on Earthquake Engineering, Istanbul, September.

Goto, H., H. Kameda, M. Sugito and N. Imanishi (1978) "Correlation on SMAC-B2 Acceleragraph Records by Digital Filter," Proceedings of the Japan Society of Civil Engineers, No.277, September (In Japanese).

Hudson, D. E. "A Comparison of Strong Motion Earthquake Data Bank for Japan and the Western United States," Proceedings of the 7th World Conference on Earthquake Engineering, Istanbul, September.

Idriss, I. M. (1978), "State of the Art -- Ground Motions," ASCE Earthquake Engineering and Soil Dynamics Conference and Exhibit, Pasadena, California, June.

Iwan, W. D. (1978), "Strong-Motion Earthquake Instrument Arrays," Proceedings of the International Workshop on Strong-Motion Earthquake Instrument Arrays, Honolulu, May.

Iwasaki, T., T. Katayama, K. Kawashima and M. Saeki (1978), "Statistical Analysis of Strong-Motion Acceleration Records Obtained in Japan," Proceedings of the 2nd International Conference on Microzonation for Safer Construction-Research and Application, November-December.

Jennings, P. C. and D. V. Helmberger (1978), "Strong-Motion Seismology," Proceedings of the 2nd International Conference on Microzonation for Safer Construction-Research and Application, San Francisco November-December.

Katayama, T., T. Iwasaki and M. Saeki (1979), "Prediction of Acceleration Response Spectra for Given Earthquake Magnitude, Epicentral Distance and Site Conditions," Bulletin of Earthquake Resistant Structure Research Center, No.11, December.

Kawashima, K. (1980), "Soil-Structure Interaction of a Highway Bridge with Use of Recorded Strong-Motion Accelerations," Proceedings of the 7th World Conference on Earthquake Engineering, Istanbul, September.

McGuire, R. K. (1974), "Seismic Structural Risk Analysis, Incorporating Peak Response Regressions on Earthquake Magnitude and Distance," Structures Publications No. 399, R74-51, Dept. of Civil Eng., Massachusetts Institute of Technology.

Okubo, T., T. Iwasaki and K. Kawashima (1980), "Dense Instrument Array Program in Public Works Research Institute for Observing Strong Earthquake-Motion," Some Recent Earthquake Engineering Research and Practice in Japan, Japanese National Committee of IAEE, Tokyo, July.

Porcella, R. L., R. B. Matthiesen, R. B. McJunkin and J. T. Ragsdale (1979), "Compilation of Strong-Motion Records the August 6, 1979 Coyote Lake Earthquake," U.S.G.S. Open-File Report 79-385 and California Division of Mines and Geology Preliminary Report 25.

Sakagami, Y., T. Okubo, T. Iwasaki and K. Kawashima (1980), "Dense Instrument Array Program of the Public Works Research Institute for Observing Strong Earthquake Motion," Proceedings of the 12th Joint Meeting, U.S. - Japan Panel on Wind and Seismic Effects, UJNR, NBS, Washington, D.C., May.

Trifunac, M.D. and A.G. Brady (1975), "On the Correlation of Seismic Intensity Scales with the Peaks of Recorded Strong Ground Motion," Bulletin of the Seismological Society of America, Vol.65, No.1, February.

Trifunac, M.D. and J.G. Anderson (1977), "Preliminary Empirical Models for Scaling Absolute Acceleration Spectral," Report No. CE 77-03, Dept. of Civil Eng., University of Southern California, Los Angeles.

Trifunac, M.D. (1977), "Forecasting the Spectral Amplitudes of Strong Earthquake Ground Motion," Proceedings of the 6th World Conference on Earthquake Engineering, New Delhi, January.

Tsuchida, H., E. Kurata and S. Hayashi (1977), "Observation of Earthquake Response of Ground with Horizontal and Vertical Seismometer Arrays," Proceedings of the 6th World Conference on Earthquake Engineering, New Delhi, January.

Tsuchida, H., S. Noda, S. Iai and E. Kurata (1980), "Observation of Earthquake Response of Ground with Horizontal and Vertical Seismometer Arrays (2nd Report)," Proceedings of the 7th World Conference on Earthquake Engineering, Istanbul, September.

Velestos, A.S. (1978), "Soil-Structure Interaction for Buildings during Earthquakes," Proceedings of the 2nd International Conference on Microzonation for Safer Construction - Research and Application, November - December.